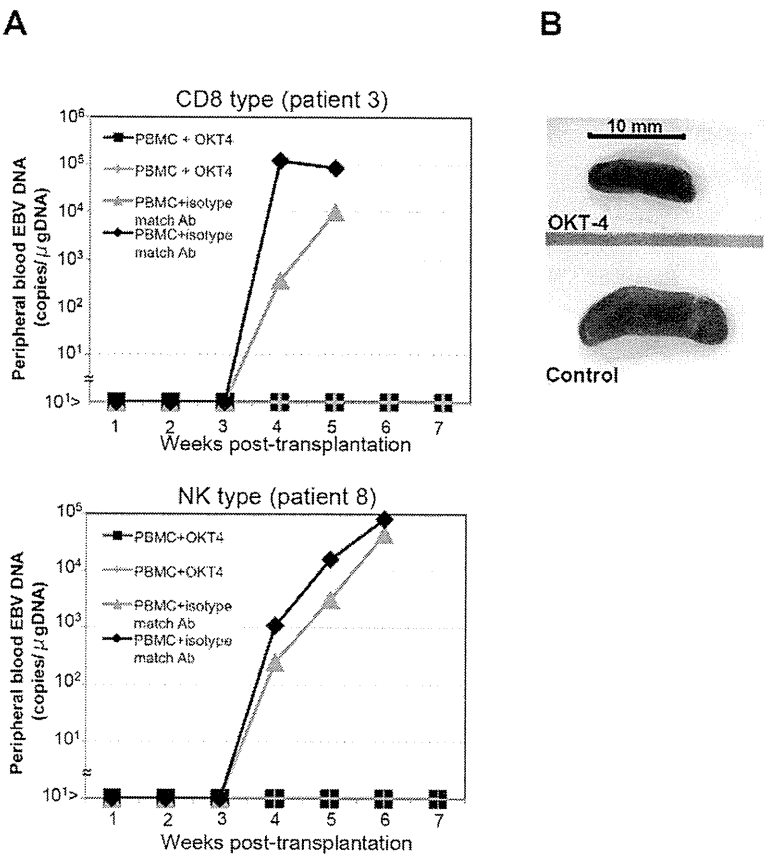

Figure 4. Suppression of the engraftment of EBV-infected T and NK cells by the OKT-4 antibody. PBMC (5×10^6 cells) isolated from the CAEBV patient 3 (CD8 type) or 8 (NK type) were injected intravenously to NOG mice. The OKT-4 antibody (100 μg/mouse) was administered intravenously on the same day of transplantation and the following three consecutive days. As a control, isotype-matched mouse IgG was injected. A. Changes in the peripheral blood EBV DNA level in the recipient mice. Results with the mice transplanted with PBMC of the patient 3 (top) and of the patient 8 (bottom) are shown. B. Photographs of the spleen of an OKT-4-treated mouse (top) and a control mouse (bottom) taken at autopsy.
doi:10.1371/journal.ppat.1002326.g004

II pattern of latent EBV gene expression after engraftment in NOG mice. Similar analyses with NOG mice engrafted with EBV-infected NK cells also showed the latency II type of EBV gene expression (data not shown).

NOG mice engrafted with EBV-infected T or NK cells produce high levels of human cytokines

In patients with CAEBV, high levels of cytokines have been detected in the peripheral blood and are thought to play important roles in the pathogenesis [20,39,40]. To test whether this hypercytokinemia is reproduced in NOG mice, we examined the levels of various human cytokines in the sera of transplanted mice using ELISA kits that can quantify human cytokines specifically. The results are shown in Figure 5B and indicate that the mice transplanted with PBMC of the patient 3 (CD8 type) or the patient 8 (NK type) contained high levels of RANTES, IFN-γ, and IL-8 in their sera.

Engraftment of EBV-infected T and B cells derived from patients with EBV-HLH in NOG mice

To extend the findings obtained from the CAEBV xenograft model to another disease with EBV^+ T/NK lymphoproliferation, we transplanted NOG mice with PBMC isolated from patients with EBV-HLH. Characteristics of the four EBV-HLH patients examined in this study and the results of transplantation with their PBMC are summarized in Table 1. EBV DNA was detected in the peripheral blood three to four weeks post-transplantation and rapidly reached the levels of 1×10^4 to 1×10^6 copies/μg DNA (results of typical experiments are shown in Figure 6A). Similar to the findings in CAEBV, EBV DNA was not detected in the recipient mice, when $CD4^+$ cell fraction was removed from PBMC (Figure 6A). Immunophenotypic analyses on the peripheral blood lymphocytes isolated from EBV-HLH patients and corresponding recipient mice revealed that cells of an identical immunophenotype ($CD3^+CD8^+CD45RO^+CD19^-CD4^-CD45RA^-CD16^-CD56^-$) were present and contained EBV DNA in both the patients and corresponding mice (Figure 6C and data not shown). The EBV DNA load observed in individual lymphocyte subsets in the patient 10 and a mouse that received his PBMC is shown as supporting data (Table S2). General condition of the recipient mice deteriorated consistently more quickly, with the loss of body weight (Figure S1), ruffling of hair, and general inactivity, than those mice engrafted with EBV-infected T or NK cells derived from CAEBV. The mice were sacrificed around four weeks post-transplantation for pathological analyses. Macroscopical observation revealed moderate to severe splenomegaly (Figure 6D) in the

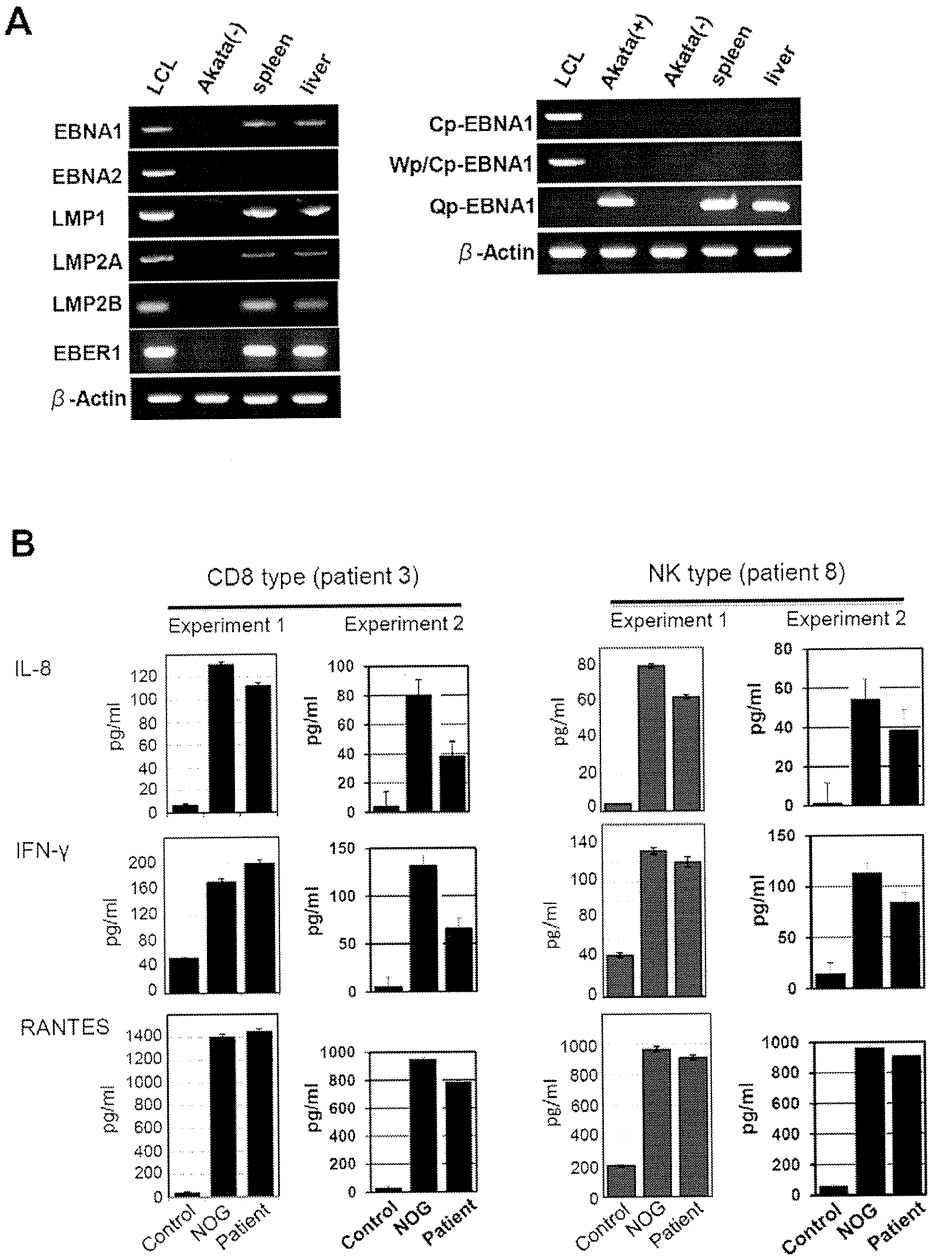

Figure 5. Analyses on the latent EBV gene expression and cytokine production in NOG mice transplanted with PBMC of CAEBV patients. A. EBV gene expression. Total RNA was purified from the spleen and liver of a mouse that received PBMC from the patient 3 (CD8 type) and applied for RT-PCR assay to detect transcripts from the indicated genes. RNA samples from an EBV-transformed B-lymphoblastoid cell line (LCL) and from EBV-negative Akata cell line were used as positive and negative controls, respectively. The primers used in the experiments are shown in Materials and Methods. B. Quantification of plasma levels of human cytokines in patients with CAEBV and corresponding recipient mice. PBMC were isolated from the patients 3 (CD8 type) and 8 (NK type) in two occasions and transplanted to NOG mice. Plasma cytokine levels of the patients were determined when their PBMC were isolated. Plasma cytokine levels of the corresponding recipient mice, prepared on each occasion of PBMC collection, were determined when they were sacrificed. Concentration of human IL-8, IFN-γ, and RANTES were measured by appropriate ELISA kits following the instruction provided by the manufacturer. Plasma samples from healthy adults were used as a control. The bars represent mean values and standard errors from triplicate measurements.
doi:10.1371/journal.ppat.1002326.g005

majority of recipient mice, and slight hepatomegaly in a limited fraction of them. A finding characteristic to these mice were massive hemorrhages in the abdominal and/or thoracic cavities, that were not seen in the mice transplanted with CAEBV-derived PBMC (Figure 6D and data not shown). These hemorrhagic lesions may reflect coagulation abnormalities characteristic to

HLH. Histopathological analyses revealed a number of $EBER^+$ cells in the spleen and the liver (Figure 6E) and quantification of EBV DNA in these tissues revealed 1.4×10^1 to 2.4×10^2 copies/μg of EBV DNA. When the tissues were examined by immunostaining and EBER ISH, the $EBER^+$ cells were shown unexpectedly to be mostly $CD45RO^-$ and $CD20^+$ in all five transplantation experiments with four different patients, indicating that the majority of EBV-infected cells in these tissues are of the B-cell lineage (Figure 6E and data not shown). $EBER^+$ large B cells were seen scattered among numerous reactive small T cells, most of which are $CD8^+$, in the tissues of the spleen, liver, lungs and kidneys. A number of macrophages were also seen in these tissues. Fractionation of mononuclear cells obtained from the liver of a mouse transplanted with PBMC of the EBV-HLH patient 10, followed by real-time PCR, detected EBV DNA (1.4×10^1 copies/μg DNA) only in the $CD19^+$ B-cell fraction. In addition, an EBV-infected B lymphoblastoid cell line, but not an EBV-positive T cell line, could be established from this liver. Thus the presence of EBV in B cells were demonstrated by three independent methods in the tissues of EBV-HLH mice. Enzyme-linked immunosorbent assay revealed extremely high levels of human cytokines, including IL-8, IFN-γ, and RANTES, in the sera of both the original patients and the recipient mice (Figure 6B). The levels of IL-8 and IFN-γ were much higher than those observed in the peripheral blood of patients with CAEBV and mice that received their PBMC. Thus, NOG mice transplanted with EBV-HLH-derived PBMC are distinct from those transplanted with CAEBV-derived PBMC in the aggressive time course of the disease, internal hemorrhagic lesions, extremely high levels of IL-8 and IFN-γ in the peripheral blood, and the presence of EBV-infected B cells in lymphoid tissues.

Discussion

The mouse xenograft models of CAEBV and EBV-HLH developed here represent the first recapitulation of EBV-associated T/NK lymphoproliferation in experimental animals. Previously, Hayashi and others inoculated rabbits with Herpesvirus papio and succeeded in the generation of T-cell lymphoproliferative disorder with pathological findings suggestive of EBV-HLH [41]. This model, however, is based on an EBV-related virus and not EBV itself, and therefore may contain features irrelevant to the original human disease. Although the CAEBV and EBV-HLH models described here exhibited some common features, including the abundant presence of EBV-infected T or NK cells in the peripheral blood, there were some critical differences between the two models, probably reflecting the divergence of the pathophysiology of the original diseases. First of all, in the EBV-HLH model mouse, EBV was detected mainly in B cells in the spleen and the liver, while it was found mainly in T cells in the peripheral blood. This makes an obvious contrast with the CAEBV model mouse, where EBV was detected in T or NK cells in both the peripheral blood and lymphoid tissues. We do not have an explanation for the apparent discrepancy in the host cell type of EBV infection between the peripheral blood and lymphoid tissues of the EBV-HLH model. It should be, however, noted that histopathology of EBV-HLH tissues has not been fully investigated and therefore it is still possible that significant number of EBV-infected B cells are present in the lymphoid tissues of EBV-HLH patients. Other differences between the two models include much higher plasma levels of IL-8 and IFN-γ more aggressive and fatal outcome, and internal hemorrhagic lesions in EBV-HLH model mice, probably reflecting the differences in the pathophysiology of the original diseases.

EBV-positive B-cell proliferation was not seen in CAEBV model mice even in long-term observation beyond twelve weeks. This seems puzzling since low but significant amount of EBV DNA was found also in $B19^+$ B-cell fraction in most patients with CAEBV. It should be noted that EBV-infected T or NK cell lines could be established relatively easily from patients with CAEBV by adding recombinant IL-2 in the medium. In contrast, establishment of EBV-infected B LCLs from these patients has been extremely difficult. In fact, we could establish B-LCLs from a few patients with CAEBV only when their PBMC were cultured on feeder cells expressing CD40 ligand. Therefore, we speculate that in the particular context of CAEBV, both in the patient and the model mouse, proliferation of EBV-infected B cells are somehow inhibited by an unknown mechanism.

Analysis on the conditions of engraftment of EBV-infected T/NK cells using these new xenograft models revealed that EBV-infected T and NK cells of the $CD8^+$ T, TCRγδT and $CD56^+$ NK lineages and cell lines derived from them require $CD4^+$ T cells for their engraftment in NOG mice. Only those EBV-infected cells and cell lines of the $CD4^+$ T lineage could engraft in NOG mice on their own. These findings suggest that some factor(s) provided by $CD4^+$ cells are essential for engraftment. Soluble factors produced by $CD4^+$ T cells may be responsible for this function and we are currently examining cytokines, including IL-2, for their ability to support the engraftment of EBV-infected T and NK cells. It is also possible that cell to cell contact involving $CD4^+$ cells is critical for engraftment. This dependence on $CD4^+$ cells represents an interesting consistency with the previous finding that engraftment of EBV-transformed B lymphoblastoid cells in *scid* mice required the presence of $CD4^+$ cells [42,43]. It has been speculated that T cells activated by an EBV-induced superantigen may be involved in the engraftment of EBV-infected B lymphoblastoid cells in *scid* mice [44]. Although a similar superantigen-mediated mechanism might also be assumed in T- and NK-cell lymphoproliferation in NOG mice, the data of TCR repertoire analyses (Figure 1C and data not shown) show no indication for clonal expansion of Vβ13 T cells that are known to be specifically activated by the EBV-induced superantigen HERV-K18. It seems therefore unlikely that this superantigen is involved in the $CD4^+$ T cell-dependent engraftment of EBV-infected T and NK cells. We expect $CD4^+$ T cells and/or molecules produced by them may be an excellent target in novel therapeutic strategies for the treatment of CAEBV and EBV-HLH. In fact, administration of the OKT-4 antibody that depletes $CD4^+$ cells in vivo efficiently prevented the engraftment of EBV-infected T cells. As a next step, we plan to test the effect of post-engraftment administration of OKT-4.

The dependence of EBV-infected T and NK cells on $CD4^+$ T cells for their engraftment in NOG mice suggests the possibility that these cells are not capable of autonomous proliferation. Consistent with this notion, EBV-infected T and NK cell lines, including that of the $CD4^+$ lineage, are dependent on IL-2 for their in vitro growth and do not engraft in either nude mice or *scid* mice when transplanted either s.c. or i.v (Shimizu, N., unpublished results). Clinically, CAEBV is a disease of chronic time course and patients carrying monoclonal EBV-infected T or NK cell population may live for many years without progression of the disease [15]. Overt malignant T or NK lymphoma usually develops only after a long course of the disease. Taking all these findings in consideration, we suppose that EBV-infected cells are not truly malignant at least in the early phase of the disease, even when they appear monoclonal. Because infection of EBV in T or NK cells is not unique to CAEBV and has been recognized also in infectious mononucleosis [45,46], the critical deficiency in

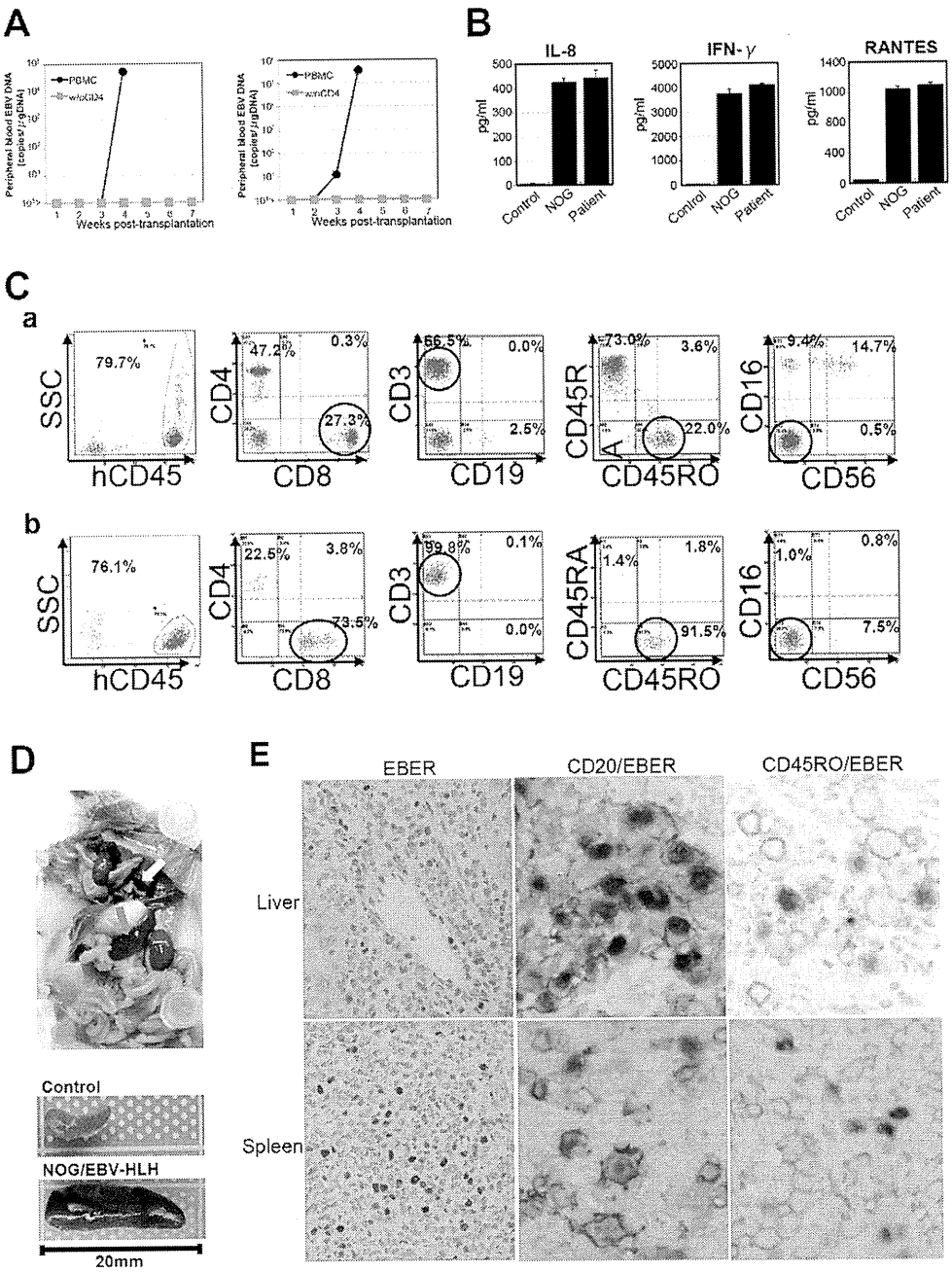

Figure 6. Engraftment of EBV-infected T and B cells in NOG mice transplanted with PBMC of patients with EBV-HLH. A. Peripheral blood EBV DNA load. Following transplantation with PBMC or PBMC devoid of $CD4^+$ cells of the patient 11, EBV DNA was measured weekly by real-time PCR. Results of two mice prepared in an experiment are shown. B. Cytokine levels in the peripheral blood of the patient 12 and a mouse that received his PBMC. The levels of IL-8, IFN-γ, and RANTES were measured by ELISA in triplicates and the means and the standard errors are shown. A plasma sample of healthy person was used as a control. C. Immunophenotypic analyses on the peripheral blood lymphocytes of the EBV-HLH patient 10 (a) and a mouse that received his PBMC (b). Lymphocytes were gated by the pattern of the side scatter and the expression of human CD45, and analyzed for the expression of the indicated markers. The circles indicate the fractions that contained EBV DNA. D. Photograph of a mouse showing splenomegaly (red arrow) and hemorrhagic lesions (yellow arrow). Spleens excised from this mouse and a control mouse are shown at the bottom. E. Photomicrographs of the tissues of mice transplanted with EBV-HLH-derived PBMC. Liver and spleen tissues of a mouse transplanted with PBMC of the patient 11 were examined by EBER-ISH (left), double staining with an anti-human CD20 monoclonal antibody and EBER-ISH (middle), and double staining with an anti-human CD45RO monoclonal antibody and EBER-ISH (right). Original magnification ×600.
doi:10.1371/journal.ppat.1002326.g006

CAEBV may be its inability to immunologically remove EBV-infected T and NK cells. In this context, it should be emphasized that EBV-infected T or NK cells usually exhibit the latency II pattern of EBV gene expression and do not express EBNA3s, that possess immuno-dominant epitopes recognized by EBV-specific T cells [47]. EBV-infected T and NK cells are thus not likely to be removed by cytotoxic T cells as efficiently as EBV-infected B cells that express EBNA3s. The reported lack of cytotoxic T cells specific to LMP2A [17], one of the few immuno-dominant EBV proteins expressed in the virus-infected T and NK cells, may therefore seriously affect the host's capacity to control their proliferation. A genetic defect in the perforin gene was recently identified in a patient with clinical and pathological features resembling CAEBV, suggesting that defects in genes involved in immune responses can result in clinical conditions similar to CAEBV [48].

Engraftment of EBV-infected T and NK cells in NOG mice was in most cases accompanied by co-engraftment of un-infected cell populations. These un-infected cells might have been maintained and induced to proliferate by certain factors produced by EBV-infected T or NK cells. Abundant cytokines produced by these cells may be responsible for this activity. It is also possible that the proliferation of these un-infected cells represents immune responses. Experiments are underway to test whether these un-infected T cells contain EBV-specific cells. These un-infected T cells might also be reacting to host murine tissues. Intravenous injection of PBMC obtained from normal humans to immunodeficient mice including NOG mice has been shown to induce acute or chronic graft versus host disease (GVHD) [49,50]. However, because much less PBMC were injected to mice in the present study as compared to those previous studies, it is not likely that major GVHD was induced in NOG mice transplanted with PBMC of patients with CAEBV or EBV-HLH.

CAEBV has been treated by a variety of regimens, including antiviral, cytocidal, and immunomodulating agents with more or less unsatisfactory results. Although hematopoietic stem cell transplantation, especially that with reduced intensity conditioning can give complete remission in a substantial number of patients [51,52], it is still desirable to develop safer and more effective treatment, possibly with pharmaceutical agents. The xenograft model of CAEBV generated in this study may be an excellent animal model to test novel experimental therapies for the disease. In fact, the OKT-4 antibody that depletes $CD4^+$ T cells in vivo gave a promising result implying its effectiveness as a therapeutic to CAEBV.

Materials and Methods

Ethics statement

Protocols of the experiments with materials obtained from patients with CAEBV and EBV-HLH and from control persons have been reviewed and approved by the Institutional Review Boards of the National Center for Child Health and Development and of the National Institute of Infectious diseases (NIID). Blood samples of the patients and control persons were collected after obtaining written informed consent. Protocols of the experiments with NOG mice are in accordance with the Guidelines for Animal Experimentation of the Japanese Association for Laboratory Animal Science and were approved by the Institutional Animal Care and Use Committee of NIID.

Patients with CAEBV and EBV-HLH

Characteristics of the nine patients with CAEBV and the four patients with EBV-HLH examined in this study are summarized in Table 1. Diagnosis of CAEBV and EBV-HLH was made on the basis of the published guidelines [19,53] and confirmed by identification of EBV-infected T or NK cells in their peripheral blood by flow cytometry and real-time PCR.

NOD/Shi-*scid*/IL2Rγ^{null} (NOG) mice

Mice of the NOD/Shi-*scid*/IL-2Rγ^{null} (NOG) strain [22] were obtained from the Central Institute for Experimental Animals (Kawasaki, Japan) and maintained under specific pathogen free (SPF) conditions in the animal facility of NIID, as described [22].

Transplantation of PBMC or their subfractions to NOG mice

PBMC were isolated by centrifugation on Lymphosepar I (Immuno-Biological Laboratories (IBL)) and injected intravenously to the tail vein of NOG mice at the age of 6–8 weeks. Depending on the recovery of PBMC, $1–4\times10^6$ cells were injected to 2 to 4 mice in a typical experiment with a blood sample. For transplantation with individual cellular fractions containing EBV DNA, $CD4^+$ T cells, $CD8^+$ T cells, and $CD56^+$ NK cells were separated with the IMag Cell Separation Systems (BD Pharmingen) following the protocol supplied by the manufacturer. To isolate γδT cells, $CD19^+$, $CD4^+$, $CD8^+$, $CD56^+$, and $CD14^+$ cells were serially removed from PBMC by the IMag Cell Separation Systems. From the remaining $CD19^-CD4^-CD8^-CD56^-CD14^-$ population, $CD3^+$ cells were positively selected by the same kit and defined as the γδT cell fraction. To transplant PBMC lacking individual immunophenotypic subsets, $CD19^+$, $CD4^+$, $CD8^+$, $CD56^+$ or $CD14^+$ cells were removed from PBMC by the IMag Cell Separation Systems and the remaining cells were injected to mice. To prepare PBMC lacking γδT cells, $CD19^+$, $CD4^+$, $CD8^+$, $CD56^+$, and $CD14^+$ cells isolated from PBMC in the process of obtaining γδT cell fraction (see above) were pooled and mixed with the $CD19^-CD4^-CD8^-CD56^-CD14^-$ cells that did not react with anti-CD3 antibody. For complementation experiments, an EBV-containing cell fraction and the $CD4^+$ cell fraction were isolated from a sample of PBMC as described above and the mixture of these two fractions were injected to NOG mice. The approximate numbers of injected cells are shown in Table 2.

Analysis of immunophenotypes and TCR repertoire expression by flow cytometry

PBMC isolated from the patients and the recipient NOG mice as described above were incubated for 30 min on ice with a mixture of appropriate combinations of fluorescently labeled monoclonal antibodies. After washing, five-color flow-cytometric analysis was carried out with the Cytomics FC500 analyzer (Beckman Coulter). The following directly labeled antibodies were used: phycoerythrin (PE)-conjugated antibodies to CD3, CD8, and TCRα/β, fluorescein isothiocyanate (FITC)-conjugated antibodies to CD3, CD4, CD8, CD19, TCRVγ9, TCRVδ2, and TCRγ/δ, and Phycoerythrin Texas Red (ECD)-conjugated antibody to CD45RO from Beckman Coulter; PE-conjugated antibodies to CD16, CD40, and CD40L, and FITC-conjugated antibody to CD56 from BD Pharmingen. TCR Vβ repertoire analysis was performed with the Multi-analysis TCR Vβ antibodies Kit (Beckman Coulter) according to the procedure recommended by the manufacturer.

Treatment of mice with the OKT-4 antibody

NOG mice were injected intravenously with 5×10^6 PBMC isolated from the CAEBV patient 3 (CD8 type) or 8 (NK type) and were subsequently injected intravenously with 100 μg of the OKT-4 antibody on the same day of transplantation. Additional

administration of the antibody was carried out by the same dose and route for the following three consecutive days. Peripheral blood EBV DNA load was then monitored every week. Mice were finally sacrificed four weeks post-transplantation and applied for pathological and virological analyses.

Quantification of EBV DNA by real time PCR and analysis of EBV gene expression by RT-PCR

Quantification of EBV DNA was carried out by real-time quantitative PCR assay based on the TaqMan system (Applied Biosystems), as described [54]. Analysis of EBV gene expression by RT-PCR was carried out as previously described with the following primers [55]. EBNA1: sense, gatgagcgtttgggagagctgattctgca; antisense, tcctcgtccatggttatcac. EBNA2: sense, agaggaggtggtaagcggttc; antisense, tgacgggtttccaagactatcc. LMP1: sense, ctctccttctcctcctcttg; antisense, caggagggtgatcatcagta. LMP2A: sense, atgactcatctcaacacata; antisense, catgttaggcaaattgcaaa. LMP2B: sense, cagtgtaatctgcacaaaga; antisense, catgttaggcaaattgcaaa. EBER1: sense, agcacctacgctgccctaga; antisense, aaaacatgcggaccaccagc. Cp-EBNA1: sense,cactacaagacctacgcctctccattcatc; anti sense, ttcggtctcccctaggccctg. Wp/Cp-EBNA1: sense, tcagagcgccaggagtccacacaaat; antisense, ttcggtctcccctaggccctg. Qp-EBNA1: sense, aggcgcgggatagcgtgcgctaccgga; antisense, tcctcgtccatggttatcac. RT-PCR primers for β-actin were purchased from Takara (Osaka, Japan).

Histopathology, EBER ISH, and immunohistochemistry

Tissue samples were fixed in 10% buffered formalin, embedded in paraffin, and stained with hematoxylin and eosin. For phenotypic analysis of engrafted lymphocytes, immunostaining for CD3, CD8 (Nichirei), CD45RO, and CD20 (DAKO) was performed on paraffin sections. EBV was detected by in situ hybridization (ISH) with EBV small RNA (EBER) probe. Immunohistochemistry and ISH were performed on an automated stainer (BENCHMARK XT, Ventana Medical Systems) according to the manufacturer's recommendations. To determine the cell lineage of EBV infected cells, paraffin sections were applied to double staining with EBER ISH and immunohistochemistry. Immediately following EBER ISH, immunostaining for CD45RO or CD20 was performed. Photomicrographs was acquired with a OLYMPUS BX51 microscope equipped with 40x/0.75 and 20x/0.50 Uplan Fl objective lens, a Pixera Penguin 600CL digital camera (Pixera), and Viewfinder 3.01 (Pixera) for white balance, contrast, and brightness correction.

Quantification of cytokines

The levels of human IL-8, IFN-γ, and RANTES in plasma samples were measured with the Enzyme-linked immunosorbent assay (ELISA) kit provided by R&D Systems following instructions provided by the manufacturer.

Accession numbers

The Swiss-Prot accession numbers for the proteins described in this article are as follows: P13501 for RANTES; P10145 for IL-8; P01579 for IFN-γ; P03211 for EBNA1; P12978 for EBNA2; P12977 for EBNA3; P03230 for LMP1; and Q66562 for LMP2. The DDBJ accession number for EBER is AJ315772.

Supporting Information

Figure S1 Changes in the body weight of NOG mice transplanted with PBMC derived from patients with CAEBV or EBV-HLH. Body weight of the five CAEBV mice shown in Figure 1A (transplanted with PBMC from the patient 1, 3, 5, and 9, and with the $CD4^+$ fraction from the patient 1, respectively) and two EBV-HLH mice shown in Figure 6A (both transplanted with PBMC from the patient 11) were recorded weekly.
(TIF)

Figure S2 Histopathological analysis of a control NOG mouse. A. a NOG mouse without xenograft. A 20-week old female NOG mouse was sacrificed and examined as a reference. No human cells are identified in these tissues. Upper panels: liver tissue was stained with hematoxylin-eosin (HE), antibodies specific to human CD3 or CD20, or by ISH with an EBER probe; the rightmost panel is a double staining with EBER and human CD45RO. Bottom panels: EBER ISH in the spleen, kidney, and small intestine. B. a NOG mouse transplanted with PBMC of a healthy EBV carrier. A six-week old female NOG mouse was transplanted with 5×10^6 PBMC isolated from a normal EBV-seropositive person and sacrificed at eight weeks post-transplantation for histological analysis. Liver and Spleen tissues were stained with HE, antibodies specific to human CD3 or CD20, or by ISH with an EBER probe. No EBER-positive cells were identified in these tissues.Original magnification is ×200 for both A and B.
(TIF)

Table S1 EBV DNA load in lymphocyte subsets of a patient with CAEBV and a corresponding mouse derived from her PBMC.
(DOC)

Table S2 EBV DNA load in lymphocyte subsets of a patient with EBV-HLH and a corresponding mouse derived from his PBMC.
(DOC)

Acknowledgments

We thank Kumiko Tanaka, Ken Watanabe, and Miki Katayama for technical assistance.

Author Contributions

Conceived and designed the experiments: KI MY NS NY SF. Performed the experiments: KI MY AN FK SI HN. Analyzed the data: KI MY AN SF. Contributed reagents/materials/analysis tools: AA TM SO MI OM JK. Wrote the paper: KI SF.

References

1. Rickinson AB, Kieff ED (2007) Epstein-Barr virus. In: Knipe DM, Howley PM, eds. Fields Virology 5. ed. Philadelphia: Lippincott Williams and Wilkins. pp 2655–2700.
2. Kieff ED, Rickinson AB (2007) Epstein-Barr virus and its replication. In: Knipe DM, Howley PM, eds. Fields Virology. Philadelphia: Lippincott Williams and Wilkins. pp 2603–2654.
3. Fujiwara S, Ono Y (1995) Isolation of Epstein-Barr virus-infected clones of the human T-cell line MT-2: use of recombinant viruses with a positive selection marker. J Virol 69: 3900–3903.
4. Watry D, Hedrick JA, Siervo S, Rhodes G, Lamberti JJ, et al. (1991) Infection of human thymocytes by Epstein-Barr virus. J Exp Med 173: 971–980.
5. Kikuta H, Sakiyama Y, Matsumoto S, Oh-Ishi T, Nakano T, et al. (1993) Fatal Epstein-Barr virus-associated hemophagocytic syndrome. Blood 82: 3259–3264.
6. Kawaguchi H, Miyashita T, Herbst H, Niedobitek G, Asada M, et al. (1993) Epstein-Barr virus-infected T lymphocytes in Epstein-Barr virus-associated hemophagocytic syndrome. J Clin Invest 92: 1444–1450.
7. Kawa-Ha K, Ishihara S, Ninomiya T, Yumura-Yagi K, Hara J, et al. (1989) CD3-negative lymphoproliferative disease of granular lymphocytes containing Epstein-Barr viral DNA. J Clin Invest 84: 51–55.
8. Jones JF, Shurin S, Abramowsky C, Tubbs RR, Sciotto CG, et al. (1988) T-cell lymphomas containing Epstein-Barr viral DNA in patients with chronic Epstein-Barr virus infections. N Engl J Med 318: 733–741.

9. Kikuta H, Taguchi Y, Tomizawa K, Kojima K, Kawamura N, et al. (1988) Epstein-Barr virus genome-positive T lymphocytes in a boy with chronic active EBV infection associated with Kawasaki-like disease. Nature 333: 455–457.
10. Ishihara S, Tawa A, Yumura-Yagi K, Murata M, Hara J, et al. (1989) Clonal T-cell lymphoproliferation containing Epstein-Barr (EB) virus DNA in a patient with chronic active EB virus infection. Jpn J Cancer Res 80: 99–101.
11. Jaffe ES (2009) The 2008 WHO classification of lymphomas: implications for clinical practice and translational research. Hematology Am Soc Hematol Educ Program 2009: 523–531.
12. Okano M (2002) Overview and problematic standpoints of severe chronic active Epstein-Barr virus infection syndrome. Crit Rev Oncol Hematol 44: 273–282.
13. Straus SE (1992) Acute progressive Epstein-Barr virus infections. Annu Rev Med 43: 437–449.
14. Kimura H (2006) Pathogenesis of chronic active Epstein-Barr virus infection: is this an infectious disease, lymphoproliferative disorder, or immunodeficiency? Rev Med Virol 16: 251–261.
15. Kimura H, Morishima T, Kanegane H, Ohga S, Hoshino Y, et al. (2003) Prognostic factors for chronic active Epstein-Barr virus infection. J Infect Dis 187: 527–533.
16. Tsuge I, Morishima T, Kimura H, Kuzushima K, Matsuoka H (2001) Impaired cytotoxic T lymphocyte response to Epstein-Barr virus-infected NK cells in patients with severe chronic active EBV infection. J Med Virol 64: 141–148.
17. Sugaya N, Kimura H, Hara S, Hoshino Y, Kojima S, et al. (2004) Quantitative analysis of Epstein-Barr virus (EBV)-specific CD8+ T cells in patients with chronic active EBV infection. J Infect Dis 190: 985–988.
18. Aoukaty A, Lee IF, Wu J, Tan R (2003) Chronic active Epstein-Barr virus infection associated with low expression of leukocyte-associated immunoglobulin-like receptor-1 (LAIR-1) on natural killer cells. J Clin Immunol 23: 141–145.
19. Henter JI, Horne A, Arico M, Egeler RM, Filipovich AH, et al. (2007) HLH-2004: Diagnostic and therapeutic guidelines for hemophagocytic lymphohistiocytosis. Pediatr Blood Cancer 48: 124–131.
20. Lay JD, Tsao CJ, Chen JY, Kadin ME, Su IJ (1997) Upregulation of tumor necrosis factor-alpha gene by Epstein-Barr virus and activation of macrophages in Epstein-Barr virus-infected T cells in the pathogenesis of hemophagocytic syndrome. J Clin Invest 100: 1969–1979.
21. Imashuku S, Hibi S, Ohara T, Iwai A, Sako M, et al. (1999) Effective control of Epstein-Barr virus-related hemophagocytic lymphohistiocytosis with immunochemotherapy. Histiocyte Society. Blood 93: 1869–1874.
22. Ito M, Hiramatsu H, Kobayashi K, Suzue K, Kawahata M, et al. (2002) NOD/SCID/gamma(c)(null) mouse: an excellent recipient mouse model for engraftment of human cells. Blood 100: 3175–3182.
23. Shultz LD, Lyons BL, Burzenski LM, Gott B, Chen X, et al. (2005) Human lymphoid and myeloid cell development in NOD/LtSz-scid IL2R gamma null mice engrafted with mobilized human hemopoietic stem cells. J Immunol 174: 6477–6489.
24. Strowig T, Gurer C, Ploss A, Liu YF, Arrey F, et al. (2009) Priming of protective T cell responses against virus-induced tumors in mice with human immune system components. J Exp Med 206: 1423–1434.
25. Watanabe S, Terashima K, Ohta S, Horibata S, Yajima M, et al. (2007) Hematopoietic stem cell-engrafted NOD/SCID/IL2Rgamma null mice develop human lymphoid systems and induce long-lasting HIV-1 infection with specific humoral immune responses. Blood 109: 212–218.
26. Yajima M, Imadome K, Nakagawa A, Watanabe S, Terashima K, et al. (2008) A new humanized mouse model of Epstein-Barr virus infection that reproduces persistent infection, lymphoproliferative disorder, and cell-mediated and humoral immune responses. J Infect Dis 198: 673–682.
27. Traggiai E, Chicha L, Mazzucchelli L, Bronz L, Piffaretti JC, et al. (2004) Development of a human adaptive immune system in cord blood cell-transplanted mice. Science 304: 104–107.
28. Melkus MW, Estes JD, Padgett-Thomas A, Gatlin J, Denton PW, et al. (2006) Humanized mice mount specific adaptive and innate immune responses to EBV and TSST-1. Nat Med 12: 1316–1322.
29. Baenziger S, Tussiwand R, Schlaepfer E, Mazzucchelli L, Heikenwalder M, et al. (2006) Disseminated and sustained HIV infection in CD34+ cord blood cell-transplanted Rag2-/-gamma c-/- mice. Proc Natl Acad Sci U S A 103: 15951–15956.
30. Zhang L, Kovalev GI, Su L (2007) HIV-1 infection and pathogenesis in a novel humanized mouse model. Blood 109: 2978–2981.
31. Dewan MZ, Watanabe M, Ahmed S, Terashima K, Horiuchi S, et al. (2005) Hodgkin's lymphoma cells are efficiently engrafted and tumor marker CD30 is expressed with constitutive nuclear factor-kappaB activity in unconditioned NOD/SCID/gammac(null) mice. Cancer Sci 96: 466–473.
32. Ishikawa F, Yoshida S, Saito Y, Hijikata A, Kitamura H, et al. (2007) Chemotherapy-resistant human AML stem cells home to and engraft within the bone-marrow endosteal region. Nat Biotechnol 25: 1315–1321.
33. Durig J, Ebeling P, Grabellus F, Sorg UR, Mollmann M, et al. (2007) A novel nonobese diabetic/severe combined immunodeficient xenograft model for chronic lymphocytic leukemia reflects important clinical characteristics of the disease. Cancer Res 67: 8653–8661.
34. Nakagawa A, Ito M, Saga S (2002) Fatal cytotoxic T-cell proliferation in chronic active Epstein-Barr virus infection in childhood. Am J Clin Pathol 117: 283–290.
35. Nagata H, Konno A, Kimura N, Zhang Y, Kimura M, et al. (2001) Characterization of novel natural killer (NK)-cell and gammadelta T-cell lines established from primary lesions of nasal T/NK-cell lymphomas associated with the Epstein-Barr virus. Blood 97: 708–713.
36. Imai S, Sugiura M, Oikawa O, Koizumi S, Hirao M, et al. (1996) Epstein-Barr virus (EBV)-carrying and -expressing T-cell lines established from severe chronic active EBV infection. Blood 87: 1446–1457.
37. Yoshioka M, Ishiguro N, Ishiko H, Ma X, Kikuta H, et al. (2001) Heterogeneous, restricted patterns of Epstein-Barr virus (EBV) latent gene expression in patients with chronic active EBV infection. J Gen Virol 82: 2385–2392.
38. Kimura H, Hoshino Y, Hara S, Sugaya N, Kawada J, et al. (2005) Differences between T cell-type and natural killer cell-type chronic active Epstein-Barr virus infection. J Infect Dis 191: 531–539.
39. Xu J, Ahmad A, Jones JF, Dolcetti R, Vaccher E, et al. (2000) Elevated serum transforming growth factor beta1 levels in Epstein-Barr virus-associated diseases and their correlation with virus-specific immunoglobulin A (IgA) and IgM. J Virol 74: 2443–2446.
40. Ohga S, Nomura A, Takada H, Ihara K, Kawakami K, et al. (2001) Epstein-Barr virus (EBV) load and cytokine gene expression in activated T cells of chronic active EBV infection. J Infect Dis 183: 1–7.
41. Hayashi K, Ohara N, Teramoto N, Onoda S, Chen HL, et al. (2001) An animal model for human EBV-associated hemophagocytic syndrome: herpesvirus papio frequently induces fatal lymphoproliferative disorders with hemophagocytic syndrome in rabbits. Am J Pathol 158: 1533–1542.
42. Veronese ML, Veronesi A, D'Andrea E, Del Mistro A, Indraccolo S, et al. (1992) Lymphoproliferative disease in human peripheral blood mononuclear cell-injected SCID mice. I. T lymphocyte requirement for B cell tumor generation. J Exp Med 176: 1763–1767.
43. Johannessen I, Asghar M, Crawford DH (2000) Essential role for T cells in human B-cell lymphoproliferative disease development in severe combined immunodeficient mice. Br J Haematol 109: 600–610.
44. Sutkowski N, Palkama T, Ciurli C, Sekaly RP, Thorley-Lawson DA, et al. (1996) An Epstein-Barr virus-associated superantigen. J Exp Med 184: 971–980.
45. Anagnostopoulos I, Hummel M, Kreschel C, Stein H (1995) Morphology, immunophenotype, and distribution of latently and/or productively Epstein-Barr virus-infected cells in acute infectious mononucleosis: implications for the interindividual infection route of Epstein-Barr virus. Blood 85: 744–750.
46. Hudnall SD, Ge Y, Wei L, Yang NP, Wang HQ, et al. (2005) Distribution and phenotype of Epstein-Barr virus-infected cells in human pharyngeal tonsils. Mod Pathol 18: 519–527.
47. Hislop AD, Taylor GS, Sauce D, Rickinson AB (2007) Cellular responses to viral infection in humans: lessons from Epstein-Barr virus. Annu Rev Immunol 25: 587–617.
48. Katano H, Ali MA, Patera AC, Catalfamo M, Jaffe ES, et al. (2004) Chronic active Epstein-Barr virus infection associated with mutations in perforin that impair its maturation. Blood 103: 1244–1252.
49. van Rijn RS, Simonetti ER, Hagenbeek A, Hogenes MC, de Weger RA, et al. (2003) A new xenograft model for graft-versus-host disease by intravenous transfer of human peripheral blood mononuclear cells in RAG2-/- gammac-/- double-mutant mice. Blood 102: 2522–2531.
50. Ito R, Katano I, Kawai K, Hirata H, Ogura T, et al. (2009) Highly sensitive model for xenogenic GVHD using severe immunodeficient NOG mice. Transplantation 87: 1654–1658.
51. Kawa K, Sawada A, Sato M, Okamura T, Sakata N, et al. (2011) Excellent outcome of allogeneic hematopoietic SCT with reduced-intensity conditioning for the treatment of chronic active EBV infection. Bone Marrow Transplant 46: 77–83.
52. Sato E, Ohga S, Kuroda H, Yoshiba F, Nishimura M, et al. (2008) Allogeneic hematopoietic stem cell transplantation for Epstein-Barr virus-associated T/natural killer-cell lymphoproliferative disease in Japan. Am J Hematol 83: 721–727.
53. Okano M, Kawa K, Kimura H, Yachie A, Wakiguchi H, et al. (2005) Proposed guidelines for diagnosing chronic active Epstein-Barr virus infection. Am J Hematol 80: 64–69.
54. Kimura H, Morita M, Yabuta Y, Kuzushima K, Kato K, et al. (1999) Quantitative analysis of Epstein-Barr virus load by using a real-time PCR assay. J Clin Microbiol 37: 132–136.
55. Nakamura H, Iwakiri D, Ono Y, Fujiwara S (1998) Epstein-Barr-virus-infected human T-cell line with a unique pattern of viral-gene expression. Int J Cancer 76: 587–594.

HIV-1 Vif-mediated ubiquitination/degradation of APOBEC3G involves four critical lysine residues in its C-terminal domain

Yasumasa Iwatani[a,b,c,1], Denise S. B. Chan[d,e], Lin Liu[d], Hiroaki Yoshii[a], Junko Shibata[a], Naoki Yamamoto[c], Judith G. Levin[f], Angela M. Gronenborn[d], and Wataru Sugiura[a,b,c]

[a]Clinical Research Center, National Hospital Organization Nagoya Medical Center, Nagoya, Aichi 460-0001, Japan; [b]University of Nagoya Graduate School of Medicine, Nagoya, Aichi 466-8550, Japan; [c]AIDS Research Center, National Institute of Infectious Diseases, Tokyo 162-8640, Japan; [d]Department of Structural Biology, University of Pittsburgh Medical School, Pittsburgh, PA 15260; [e]Department of Chemistry, University of Hong Kong, Pokfulam Road, Hong Kong, China; and [f]Laboratory of Molecular Genetics, Eunice Kennedy Shriver National Institute of Child Health and Human Development, National Institutes of Health, Bethesda, MD 20892

Edited by John M. Coffin, Tufts University School of Medicine, Boston, MA, and approved September 24, 2009 (received for review June 16, 2009)

During coevolution with the host, HIV-1 developed the ability to hijack the cellular ubiquitin/proteasome degradation pathway to counteract the antiviral activity of APOBEC3G (A3G), a host cytidine deaminase that can block HIV-1 replication. Abrogation of A3G function involves the HIV-1 Vif protein, which binds A3G and serves as an adapter molecule to recruit A3G to a Cullin5-based E3 ubiquitin ligase complex. Structure-guided mutagenesis of A3G focused on the 14 most surface-exposed Lys residues allowed us to identify four Lys residues (Lys-297, 301, 303, and 334) that are required for Vif-mediated A3G ubiquitination and degradation. Substitution of Arg for these residues confers Vif resistance and restores A3G's antiviral activity in the presence of Vif. In our model, the critical four Lys residues cluster at the C terminus, opposite to the known N-terminal Vif-interaction region in the protein. Thus, spatial constraints imposed by the E3 ligase complex may be an important determinant in Vif-dependent A3G ubiquitination.

structure model | deaminase | antiviral

Human APOBEC3G (hA3G), is a host cytidine deaminase that has two homologous Zn cluster (H/C)XE(X)$_{23\sim28}$CXXC-containing domains [reviewed in (1, 2)]. Sheehy et al. (3) identified hA3G as the cellular factor that blocks HIV-1 replication in certain T cells (e.g., H9 or primary T-cell lymphocytes) in the absence of the viral protein Vif. Cellular expression of A3G results in its incorporation into *vif*-deficient HIV-1 particles, whereas the presence of A3G in wild-type (WT) virions is dramatically reduced by Vif-induced degradation via the ubiquitination-proteasome pathway before virion assembly and release (4–9). There is also evidence for other degradation-independent mechanisms (10, 11 and references therein).

In the absence of Vif, virion-encapsidated A3G causes extensive C-to-U mutations in synthesized minus-strand viral DNA and also physically blocks reverse transcription, rendering the virus noninfectious [(12–14) and reviewed in (11)]. Thus, given Vif's critical role in eliminating A3G function, it may be viewed as one of the most attractive pharmacologic targets for an anti-HIV drug aimed at restoring the activity of the intrinsic antiviral factor A3G in the context of HIV-1 infection. Indeed, such efforts have already begun. A recent report describes the small molecule inhibitor (RN-18) that increases cellular levels of A3G and incorporation of A3G into virions in a Vif-dependent manner (15).

Ubiquitination is catalyzed by a complex cascade system consisting of the ubiquitin (Ub)-activating (E1), Ub-conjugating (E2), and Ub-ligating (E3) enzymes (16, 17). Among these enzymes, the E3 class represents a diverse family of protein complexes, responsible for the selection of the target proteins. In particular, the Cullin-based E3 enzymes belong to the family of RING E3 Ub ligases that contain three main components: a Cullin (Cul1, 2, 3, 4a, 4b, 5, and 7), an adaptor, and a substrate receptor (18). In the Vif-A3G system, these proteins are Cul5, elongin B/C (EloB/C), and Vif, respectively. Cullin functions as a molecular scaffold on which the adaptor protein and receptor assemble to bring a specific substrate in close proximity to the E2 Ub-conjugating enzyme. The substrate receptor determines the specificity of the protein to be degraded and binds to Cullin through the adaptor protein. The E2-conjugating enzyme transfers multiple Ub molecules to the substrate, targeting it for degradation by the proteasome.

In general, the first Ub is typically conjugated to an ε-amino group of an internal Lys in the substrate (in this case, A3G). HIV-1 Vif, serving as the substrate receptor, facilitates ubiquitination of A3G by simultaneously binding to the Cul5-EloB/EloC-Rbx-E2 complex, thereby mimicking the function of cellular suppressor of cytokine signaling (SOCS) box proteins (9, 19–21). The SOCS box-like motif of Vif is highly conserved among primate lentiviruses and contains a BC box, as well as a Cullin box. The BC box motif creates a hydrophobic interface for binding to EloC. The Cullin box has a specific site for binding to Cul5, which involves an interaction between the highly conserved HCCH zinc-binding motif in Vif and the N-terminal domain (NTD) of Cul5 (22, 23).

Interestingly, it has been reported that Vif contains three sequence motifs for binding to A3G: $_{12}$QVDRMR$_{17}$; $_{40}$YRHHY$_{44}$; and $_{69}$YXXL$_{72}$ (24–26). The region in A3G responsible for binding to HIV-1 Vif was initially identified by comparative studies of the species specificity of A3G degradation by Vif. Thus, a single amino acid difference in hA3G, Asp at position 128 versus Lys in the A3G of African green monkeys ($A3G_{agm}$), determines species specificity by influencing Vif-A3G binding (27–30). Furthermore, extensive site-directed mutagenesis revealed that the $_{128}$DPD$_{130}$ motif of A3G, located near the first Zn cluster, is crucial for direct binding to HIV-1 Vif. It is of interest that this motif is just downstream of residues $_{124}$YYFW$_{127}$, which are involved in A3G's ability to bind nucleic acids (31).

Author contributions: Y.I., D.S.B.C., J.G.L., A.M.G., and W.S. designed research; Y.I., D.S.B.C., L.L., H.Y., and J.S. performed research; Y.I. contributed new reagents/analytic tools; Y.I., D.S.B.C., L.L., N.Y., J.G.L., A.M.G., and W.S. analyzed data; and Y.I., D.S.B,C., J.G.L., and A.M.G. wrote the paper.

The authors declare no conflict of interest.

This article is a PNAS Direct Submission.

Freely available online through the PNAS open access option.

[1]To whom correspondence should be addressed at: Clinical Research Center, National Hospital Organization Nagoya Medical Center, 4-1-1 San-no-maru, Naka-ku, Nagoya, Aichi 460-0001, Japan. E-mail: iwataniy@nnh.hosp.go.jp.

This article contains supporting information online at www.pnas.org/cgi/content/full/0906652106/DCSupplemental.

MICROBIOLOGY

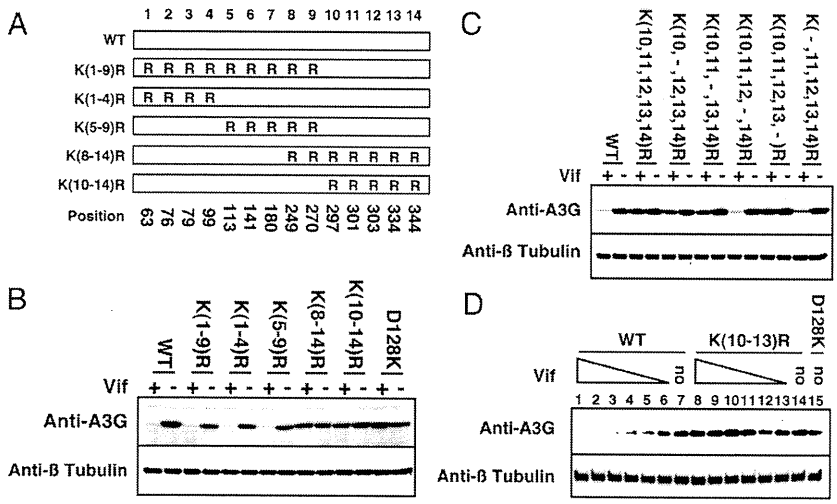

Fig. 1. Lys to Arg substitution mutations conferring A3G resistance to HIV-1 Vif-dependent degradation. (*A*) WT A3G and mutants. Numbers 1 to 14, shown above the diagram, refer to the 14 Lys residues illustrated in Fig. S2 [i.e., at positions 63, 76, 79, 99, 113, 141, 180, 249, 270, 297, 301, 303, 334, and 344 (K1–14), respectively (position numbers indicated below the figure)]. Five mutants have Arg substitutions in K1–9, 1–4, 5–9, 8–14, and 10–14 and were designated as K (1–9)R, K(1–4)R, K (5–9)R, K(8–14)R, and K(10–14)R, respectively. (*B*) and (*C*) Vif-dependent degradation of A3G mutants. 293T cells were transfected with or without pcDNA-HVif plus the indicated A3G expression plasmid. The amounts of cellular A3G from cells transfected with or without the Vif-expressing plasmid were compared by Western blot analysis using anti-A3G antibody. In (*B*), D128K, a defective A3G that does not bind Vif, was used as a positive control. (*D*) Effect of increasing levels of Vif expression on degradation of WT A3G and A3G mutant K(10, 11, 12, 13)R. Two micrograms of each A3G expression plasmid was used. For Vif expression, pcDNA-HVif/pcDNA 3.1 (-) plasmids (8 μg) were used at the following ratios: 8:0 (lanes 1, 8, 15); 1:1 (lanes 2 and 9); 3:5 (lanes 3 and 10); 1:3 (lanes 4 and 11); 1:15 (lanes 5 and 12); 1:79 (lanes 6 and 13); and 0:8 (lanes 7 and 14). Anti-ß-tubulin antibody was used as a control.

The information available thus far concerning the interaction between Vif and A3G in the Ub ligase complex suggests that there may be a specific mechanism for Ub conjugation of the A3G protein. Yet, despite our knowledge that the participants interact with each other in the EloB/C-Cul5-Vif-A3G complex, the details of how the complex dictates A3G polyubiquitination and subsequent degradation remain unclear. In part, this is due to the lack of complete structural information about the A3G and Vif proteins and the complex they form. Our approach to this problem was to construct a structural model of hA3G for testing which Lys residues may serve as targets for ubiquitination. Based on the structural model we selected 14 surface-exposed Lys and established that only four of these residues (Lys-297, 301, 303, and 334) in the C-terminal domain (CTD) are essential for Vif-induced degradation of A3G. In addition, we demonstrated that a "super" A3G (S-A3G) with all of these four residues mutated to Arg was resistant to degradation by Vif and was able to block replication of WT HIV-1. Taken together, our results provide insights into the determinants governing Vif-mediated A3G inactivation and should stimulate and aid efforts to develop antiviral strategies that focus on disruption of the Vif-A3G interaction.

Results

The A3G Model Shows 14 Lys Residues with Substantially Exposed ε-Amino Groups. The goal of the present study was to identify Lys residues in hA3G that become ubiquitinated in a Vif-dependent manner, resulting in subsequent degradation by the proteasome pathway. In general, during polyubiquitination, the first ubiquitin is typically conjugated to an ε-amino group of an exposed Lys within the target protein (16). For hA3G, the amino acid sequence contains 20 Lys residues (Fig. S1), 14 of which are completely accessible on the surface in a model structure (Fig. S2). Our model structure was based on the X-ray structures of the A3G catalytic domain (32) and the related homodimeric A2 protein (33) and was generated to guide our selection of the most solvent accessible Lys residues. Homology models for the NTD and CTD were generated using the program Modeller (http://salilab.org/modeller) (34) and the relative positioning of the domains in the A3G model was based on the arrangement of the monomeric A2 proteins in the homodimer. The most exposed Lys residues were found at positions 63, 76, 79, 99, 113, 141, 180, 249, 270, 297, 301, 303, 334, and 344, and are highlighted in blue in the amino acid sequence of hA3G (Fig. S1). In the following discussion they are designated as K1–14, respectively.

Arg Substitutions for Lys-297, 301, 303, and 334 Render A3G Resistant to Vif-Mediated Degradation. In an effort to identify which Lys residue(s) may be responsible for A3G ubiquitination, Arg substitutions were made at the selected 14 positions in A3G and mutants were assayed for intracellular degradation. In particular, we tested whether HIV-1 Vif enhanced degradation ("Vif sensitivity") of A3G was affected. Initially, 14 point mutants were constructed and each mutant remained Vif-sensitive (Fig. S3). This suggested that most likely, more than one residue might be required for conversion to a Vif-resistant phenotype.

To address this question (i.e., whether several Lys residues may be involved), a series of mutants was constructed, each containing changes for a number of Lys residues (Fig. 1). Five mutants, K (1–9)R, K(1–4)R, K (5–9)R, K(8–14)R, and K(10–14)R, with Arg substitutions at positions K1–9, 1–4, 5–9, 8–14, and 10–14, respectively, were generated (Fig. 1*A*) and the presence of A3G was probed by Western blot analysis (see legend to Fig. 1). As expected, WT A3G was not detectable when co-expressed with HIV-1 Vif (Vif-sensitive), while the level of the D128K A3G mutant protein that lacks the ability to bind HIV-1 Vif (27–30) was unchanged in the presence of Vif (Vif-resistant) (Fig. 1*B*). The K (1–9)R, K(1–4)R, and K(5–9)R mutants were sensitive to Vif, i.e., they behaved like WT A3G in this assay. In contrast, protein levels of the K(8–14)R and K(10–14)R mutants were unaffected (i.e., Vif-resistant) (Fig. 1*B*). This suggested that all five Lys residues from 10 through 14, or a subset thereof, were critical for mediation of Vif-dependent ubiquitination.

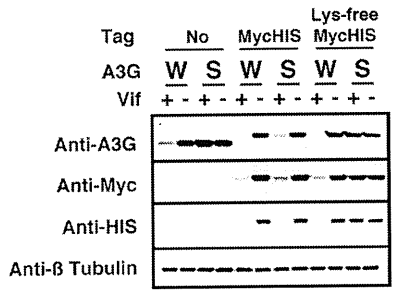

Fig. 2. Effect of a MycHIS tag at the C-terminal end of A3G. WT A3G (W) or S-A3G (S) without a tag (No), with a MycHIS tag or the Lys-free MycHIS tag were expressed in the presence or absence of Vif in 293T cells. A3G was detected by Western blot with anti-A3G antibody (Anti-A3G), anti-Myc tag monoclonal antibody (Anti-Myc), or anti-(His_6) tag antibody (Anti-HIS).

To resolve this point, a second series of A3G mutants with different permutations of the four substitutions in residues 10–14 was evaluated. Only K(10, 11, 12, 13)R was completely Vif-resistant, although K(10, 12, 13, 14)R and K(10, 11, 13, 14)R were partially resistant (Fig. 1*C*). This result demonstrated that Lys residues 10, 11, 12, and 13 are critical determinants of HIV-1 Vif-dependent ubiquitination of A3G, since Arg substitutions in these residues abolished Vif sensitivity, Furthermore, three substitutions within the four residues conferred varying degrees of A3G sensitivity to Vif. To corroborate these conclusions, we compared the amounts of A3G WT and K(10–13)R proteins for varying ratios of pcDNA-HVif/pcDNA 3.1 (-). While significant WT A3G protein was present at low Vif concentrations (Fig. 1*D*, lanes 4–6), no difference in protein amounts was observed for the K(10–13)R mutant at every concentration of Vif that was tested (Fig. 1*D*, lanes 8–13). Thus, K(10–13)R is resistant to Vif-mediated degradation and we will refer to mutant K(10–13)R as "super" A3G (S-A3G) below. We also observed S-A3G Vif resistance in nonpermissive SupT1 T-cell lymphocytes (Fig. S4).

The Additional C-Terminal Tag of A3G Can Mediate Ubiquitination-Induced Proteasomal Degradation. In an initial phase of this study, quite unexpectedly, we found that an A3G mutant with all 14 Lys residues changed to Arg and also having a C-terminal tag was sensitive to Vif-dependent degradation. This surprising result prompted us to test whether the two Lys residues in the C-terminal A3G tag (MycHIS) might become ubiquitinated. We therefore constructed A3G expression plasmids with a Lys-free MycHIS tag and compared the Vif sensitivity of this construct with that of untagged and conventional MycHIS tagged WT and S-A3G plasmids. As clearly seen in Fig. 2, S-A3G protein levels were similar in the absence or presence of HIV-1 Vif. In contrast, the addition of the C-terminal MycHIS tag rendered S-A3G (S) susceptible to the presence of Vif, exhibiting behavior very similar to that of WT A3G. This was reversed when the Lys-free MycHIS version of S-A3G was used. In this case, complete resistance to Vif-dependent A3G degradation was noted. These findings demonstrated that the two Lys in the C-terminal tag can serve as ubiquitination sites. Note that identical protein levels were detected irrespective of the type of antibodies (anti-A3G, anti-Myc or anti-HIS antibodies) used for detection (Fig. 2).

The dependence of A3G polyubiquitination on Vif was investigated by expressing the Lys-free MycHIS tagged A3G in 293T cells. The results showed that no polyubiquitinated S-A3G was detectable, whereas Vif-dependent WT A3G polyubiquitination was clearly observed (Fig. S5). This demonstrates that S-A3G's resistance to Vif-dependent degradation was due to its inability to be polyubiquitinated, presumably as a consequence of the four Lys mutations.

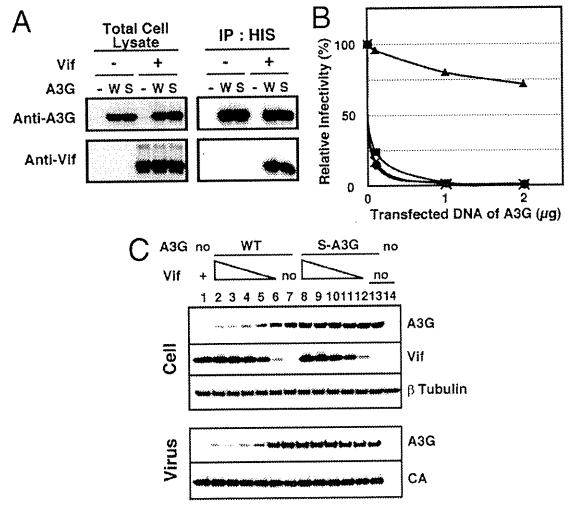

Fig. 3. Effect of incorporation of the K(10, 11, 12, 13)R mutant (S-A3G) into WT or *vif*-deficient virions on infectivity in a single-cycle replication assay. (*A*) 293T cells were cotransfected with pcDNA-HVif and either empty (-), WT (W), or S-A3G (S) plasmids having the Lys-free MycHIS tag, using the procedures described in *Materials and Methods*. The MycHIS-tagged proteins were analyzed either directly (*Left*) as "Total Cell Lysate" or following pull-down (binding of the HIS tag to TALON resin) (*Right*) by immunoblotting with the indicated antibodies. (*B*) Virus infectivity; 293T cells were cotransfected with (*i*) pNL4–3 and either WT (▲) or S-A3G (●) expression plasmids or (*ii*) pNL4–3*vif*(-) and either WT (■) or S-A3G (crosses) expression plasmids, using 0, 0.1, 1, or 2 μg of DNA. Where appropriate, the amounts of DNA added for each of the expression plasmids were adjusted with empty vector pcDNA 3.1 (-) to a total of 2 μg. Infectivity values are given relative to the values for 0 μg of the expression plasmids and were set at 100%. (*C*) Analysis of intracellular expression (Cell) and incorporation of WT and S-A3G into virions (Virus) by Western blot. Virions were produced by transfection of pNL4–3 WT/pNL4–3*vif*(-) plus either A3G WT, S-A3G expression plasmid or pcDNA 3.1(-) (shown as "no"). The ratios of pNL4–3 WT to pNL4–3*vif*(-) were as follows. 1:0 (lanes 1, 2 and 8), 1:1 (lanes 3 and 9), 1:3 (lanes 4 and 10), 1:7 (lanes 5 and 11), 1:79 (lanes 6 and 12), and 1:0 (lanes 7 and 13). The intracellular levels of β-tubulin and Vif and the CA level in virions were detected by anti-β-tubulin, anti-Vif, and anti-CA antibodies, respectively.

S-A3G Displays Normal Vif Binding. Abrogation of Vif binding by A3G could also confer resistance to Vif-dependent degradation, as was observed for the D128K mutant (27–30). It therefore seemed prudent to determine whether Arg substitutions at A3G residues 297, 301, 303, and 334 would in any way interfere with A3G's ability to bind Vif. We expressed WT and S-A3G (bearing the Lys-free MycHIS tag) in the presence of the proteasome inhibitor MG132 (2 μM), with or without Vif. Intracellular A3G-Vif complexes were pulled down with Talon beads via the HIS portion of A3G's C-terminal tag and the complexes were detected by either anti-A3G or anti-Vif antibodies (Fig. 3*A*). Coprecipitated complexes of WT or S-A3G contained very similar amounts of Vif, indicating that no impairment of Vif binding resulted from the mutations in S-A3G. As expected, no Vif was detected in the controls.

S-A3G Inhibits HIV-1 Infection. To assess the implications of S-A3G's resistance toward Vif-dependent proteasomal degradation, we tested whether S-A3G exhibited any antiviral activity against HIV-1. To this end, we compared the infectivity of WT and *vif*-deficient HIV-1 in the presence of WT or S-A3G in a single-round replication assay. Since A3G expression levels and the extent of the antiviral effect vary for different virus-producer

cell lines (35, 36), we measured infectivity in this assay as a function of the amount of transfected DNA. Comparing infectivity for a given amount of A3G to infectivity in the absence of A3G was termed "relative infectivity." Interestingly, using 0.1 and 2.0 μg WT A3G DNA for transfection reduced the infectivity of *vif*-deficient HIV-1 to 24 and 0.8%, respectively, while only marginally affecting the infectivity of WT HIV-1 (95 and 71% with 0.1 and 2.0 μg, respectively) (Fig. 3*B*). In contrast, S-A3G suppressed the infectivity of *vif*-deficient as well as WT HIV-1 significantly, consistent with its Vif-resistant phenotype. Furthermore, we could show that a deaminase-deficient version (E259Q) of S-A3G had less antiviral activity than S-A3G against WT and *vif*-deficient HIV-1 (Fig. S6). Note, too, that in the absence of Vif, E259Q mutants derived from WT and S-A3G had the same levels of inhibitory activity (Fig. S6*B*). Collectively these results suggest that the catalytic activity and the antiviral function of S-A3G and WT A3G are equivalent.

To determine whether the inhibitory effect of S-A3G on WT HIV-1 infectivity is correlated with a defect in efficient incorporation of S-A3G into virus particles, we analyzed the amounts of intracellular A3G and A3G packaged into virions as a function of Vif expression (i.e., by transfecting different ratios of pNL4–3/pNL4–3 *vif*(-) together with either WT A3G or S-A3G) (Fig. 3*C*). As Vif expression was increased, the steady state levels of intracellular WT A3G were decreased (Cell, lanes 2–6), while the levels of S-A3G protein were not affected (Cell, lanes 8–12). Concomitant with the decrease in protein levels of intracellular WT A3G, its incorporation into virions was also reduced (Virus, lanes 2–6), while under identical experimental conditions, S-A3G packaging was not significantly affected (Virus, lanes 8–12). These findings demonstrate that S-A3G incorporation into HIV-1 virions is independent of Vif. Therefore, efficient packaging of S-A3G into HIV-1 virus particles occurs and allows S-A3G to exert its inhibitory effect on viral infectivity.

The Critical Residues Involved in Vif-Mediated A3G Degradation Cluster at the C Terminus of the Protein. Identification of the Lys residues crucial for Vif-mediated A3G degradation in conjunction with the molecular model for the protein allowed us to determine their location. All 14 candidate Lys are displayed on the model in Fig. 4. As can be readily observed, the critical residues involved in ubiquitination and proteasomal degradation of A3G (i.e., Lys 297, 301, 303, and 334) cluster in one region of the molecule. This area is located at the opposite end of the known interaction region with Vif (D128, P129, and D130) (31). Interestingly, the critical Lys residues are also close to the C terminus of the polypeptide chain, with K334 located within approximately 13Å. Note that this model also positions the Lys residues of the MycHIS tag in the same general area (Fig. 4*A*, green), possibly explaining our findings regarding Vif-sensitivity of MycHIS tagged S-A3G.

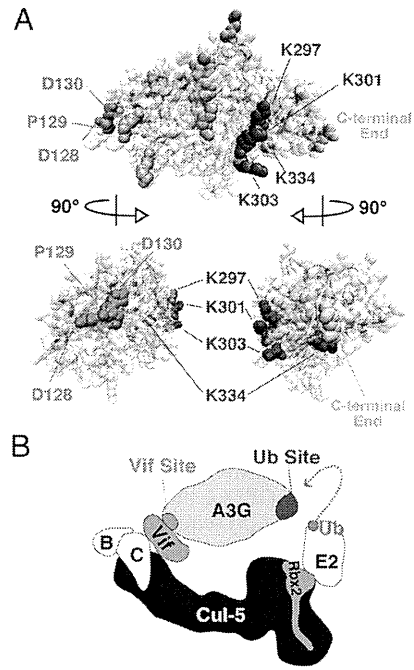

Fig. 4. Region of A3G involved in ubiquitination around Lys residues 297, 301, 303, and 334 and Vif binding mapped onto the structural model. (*A*) Side and 90°-rotated (counterclockwise or clockwise) views of the model in surface representation. Lys residues 297, 301, 303, and 334 are shown in blue, all of the other Lys in cyan, the C-terminal end of A3G in green, and residues D128, P129, and D130 responsible for Vif-binding in red. (*B*) Cartoon illustration of the A3G/Vif/ElonginB/C/Cul-5/Rbx2/E2 complex. The ubiquitination sites on the A3G substrate are marked in blue and the Vif binding site in orange.

Discussion

The goal of the present study was to provide information about HIV-1 Vif-induced degradation of hA3G, in particular the initial polyubiquitination step (i.e., conjugation of Ub to Lys residues in A3G). Using structure-based mutagenesis as our experimental approach, we identified four Lys residues at positions 297, 301, 303, and 334 in the CTD of A3G that are critical for Vif-dependent degradation. Mutation of these residues to Arg generated a protein, S-A3G, which is resistant to intracellular degradation mediated by HIV-1 Vif. Importantly, the interaction between WT A3G and S-A3G with Vif is very similar and S-A3G is incorporated into WT and *vif*-deficient viral particles to the same extent. In addition, S-A3G dramatically reduces the infectivity of both WT and *vif*-deficient HIV-1 (Fig. 3).

To evaluate ubiquitination of A3G at the structural level, we constructed a model of full-length A3G (Fig. S2) based on the crystal structures of the A3G catalytic domain (32) and A2 (33), yielding a domain arrangement of N- and C-terminal domains similar to the individual subunits in homodimeric A2. The structures of the individual domains are very similar to those of other cytidine deaminases and are characterized by a five-stranded mixed beta sheet and five alpha helices. The current CTD of our model is not substantially different from the CTD structures that were recently determined by X-ray crystallography and NMR (32, 37–39). Since we created and used our homology model to guide the current mutagenesis, several other models of A3G have become available (40, 41). Most exhibit a domain disposition similar to the one shown here. Very recently a divergent model has been proposed in which the domains are rotated and the ß-sheet arrangement seen in A2 is not retained (39). Although in this model the details in location of Lys residues will vary, the fact that the Vif interaction site and the critical C-terminal Lys cluster are found at opposite ends of the molecule is still valid.

Even though mutation of these four Lys to Arg residues is the minimum requirement for blocking ubiquitination of A3G, it is of interest to evaluate whether any of these four residues is more favored than others as targets for modification. Both A3G mutants K(10, -, 12, 13, 14)R and K(10, 11, -, 13, 14)R are only partially resistant to ubiquitination compared with A3G K(10, 11, 12, 13, -)R, the molecule termed S-A3G (Fig. 1*C*). This suggests that Lys-301 and Lys-303 (K11 and K12, respectively) are used to a lesser extent than Lys-297 and Lys-334 (K10 and K13, respectively) for ubiquitination. Indeed, it is entirely possible that Lys-297 and Lys-334 represent the two required Lys for Vif-induced A3G degradation and that the two Lys that follow Lys 297, Lys 301 one turn further down the helix and Lys-303 in the following helix, may be able to partially substitute as targets

(Fig. S1). Interestingly, Lys-297 and 334, the most sensitive of the four residues, are highly conserved among primate A3Gs compared with Lys-301 and 303 (Fig. S7).

Surprisingly, in a mutagenesis study similar to the work reported here, Dang et al. found that mutation of all 20 Lys residues in A3G to Arg had no effect on Vif-induced degradation of A3G (42). In an additional test of our model, we also mutated all 20 Lys in A3G (A3G 20K/R) and assayed Vif sensitivity, as well as antiviral activity. Our data showed that like K(1–14)R (the mutant in which all surface-exposed Lys were changed to Arg), A3G 20K/R, 19K/R, and 17K/R were also resistant to Vif-dependent degradation (Fig. S8*A*). Moreover, the results indicated that A3G 20K/R, like S-A3G, can suppress virus infectivity even in the presence of Vif (Fig. S8*B*). These findings differ from the report by Dang et al. (42), but the reasons for the apparent discrepancy between our results and those published previously are not clear.

In contrast to the residues that are involved in ubiquitination of A3G, amino acids implicated in Vif binding are located in the NTD (43) within the $_{128}$DPD$_{130}$ motif (31, 43) that is embedded in the $_{126}$FWDPDYQ$_{132}$ (25) sequence in a loop preceding helix 4, which protrudes out from the overall structure (Fig. S2). Significantly, this motif resides on a site opposite to the location of residues involved in ubiquitination in the overall structure (Fig. 4*A*). Consistent with the model, Vif binding by WT A3G and S-A3G are similar, as evidenced by the coimmunoprecipitation results (Fig. 3*A*).

In the absence of an experimentally determined three-dimensional structure of HIV-1 Vif, predictions about the configuration of the A3G-Vif-ElonginB/C-Cullin-5 E3 Ub ligase complex can only be speculative. Based on the Skp1-Cul1-Rbx1-F box^{Skp2} (SCF) structure (44) we propose the following scenario for positioning A3G in the complex (Fig. 4*B*). It is generally accepted that the cullins provide a rigid scaffold for positioning donor and acceptor proteins in the ubiquitination reaction catalyzed by E3. Indeed, mutants in Cul 1 that were designed to eliminate the integrity of the scaffold are deficient in Ub catalysis (44). Moreover, studies on the SCF complex suggested that positioning can explain Lys specificity, i.e., which Lys are the targets for ubiquitination. For example, IkB and SnoN, which are among the few ubiquitinated proteins that have been characterized in detail, are ubiquitinated at specific Lys residues by the SCF and SCF-like complexes consistent with their structural positioning (45, 46).

Similarly, our data suggest that Vif-dependent ubiquitination of A3G in the context of a Cul5-based complex specifically occurs on a site that is located at the end of the protein opposite to the region involved in Vif binding. Thus, spatial constraints imposed by the E3 Ub ligase complex involving Cul5 may be an important determinant for Vif-dependent A3G ubiquitination. It is of interest that HIV-2 and SIV$_{mac}$ Vif proteins target the same Lys residues in hA3G as HIV-1 Vif (Fig. S9). Thus, all three Vif proteins might form complexes with similar structural constraints.

Based on the SCF structural data (45, 46), it seems reasonable to assume that the distance between the E2 active-site Cys and the Ub-modification site on the substrate also plays an important role in activity (44, 47). The average distance in the SCF complexes is approximately 60 Å (44, 47). In the present A3G model, the distance between the $_{128}$DPD$_{130}$ cluster and the critical Lys residues ranges from 45Å to 60Å, very similar to the distance between the E2 active-site Cys and the substrate-binding site within the Cul 5-EloB/C-Vif-Rbx2-E2 complex. Interestingly, in a recent study by Russell et al. on A3F, the Vif binding region was identified as amino acids 283 to 300 (25). Reference to the A3G structural model suggests that the A3F Vif-binding site corresponds to the A3G ubiquitination region where Lys-297, 301, and 303 are located.

In summary, using model-guided mutagenesis, we have identified four Lys residues in the CTD of A3G that are required for Vif-mediated polyubiquitination and degradation. We show that substitution of four critical Lys to Arg (S-A3G) confers Vif-resistance to A3G and restores A3G's antiviral activity irrespective of Vif. At present, since no polymorphisms at these residues have been reported for hA3G, the natural appearance of A3G variants such as S-A3G is highly unlikely. However, identification of a specific target molecule that removes Vif's inhibitory effect on A3G could advance efforts to develop anti-HIV-1 drugs. Similarly, efforts to design specific screening assays for anti-Vif compounds in vitro will benefit from further characterization of the Vif-A3G interplay with respect to proteasomal degradation.

Materials and Methods

Construction of A3G Structure Model. A homology model of A3G was created based on sequence alignment (automated and adjusted by hand) and subsequent use of the program Modeller (http://salilab.org/modeller) (34) with the crystal structure of the A3G catalytic domain (32) (PDB accession code 3E1U) as the template for the individual NTD and CTD domains. The relative positioning of the NTD and CTD of the template was carried out by superimposing the separated domains onto the crystal structure of A2 (33) (PDB accession code 2NYT). The choice of interface between the two halves of A3G was guided by energy considerations of the final models. The current model in which the beta strands form the dimer interface is energetically more favorable than an alternative one with an alpha helical domain interface.

Plasmids and Antibodies. The plasmids and antibodies used in this work are described in the *SI Text*.

Coimmunoprecipitation Assays. To assess Vif-A3G interaction in vivo, a assay was performed. Briefly, 293T cells were cotransfected with an A3G plasmid having a Lys-free MycHIS tag and with pcDNA-HVif. Thirty-six hours post transfection, the cells were incubated for 12 h with 2 μM MG132, a proteasome inhibitor (Sigma). The presence of MG132 makes it possible to detect WT A3G binding to Vif, since the usual proteasomal degradation is blocked. The cells were harvested and then lysed in lysis buffer (150 mM NaCl, 1 mM EDTA, PBS, 1% Triton X-100, 10 μg/mL of RNase A) plus a protease inhibitor mixture (Sigma). TALON beads (Clontech), which bind His, were used to pull down tagged A3G and were washed with lysis buffer. The complex was analyzed by Western blot with anti-A3G rabbit serum or anti-Vif antibody.

Assays for Vif-Dependent Degradation of A3G, Infectivity in LuSIV Cells and Incorporation of A3G Into Virions. These experiments were performed as reported previously (48).

ACKNOWLEDGMENTS. This work was supported in part by a grant-in-aid for Scientific Research from the Ministry of Education, Culture, Sports, Science and Technology, Japan (to Y.I.); National Institutes of Health Grant GM082251 (to A.M.G); the Intramural Research Program of the National Institutes of Health, Eunice Kennedy Shriver National Institute of Child Health and Human Development (to J.G.L.); and a grant-in-aid for AIDS Research from the Ministry of Health, Labor, and Welfare, Japan (to W.S.).

1. Holmes RK, Malim MH, Bishop KN (2007) APOBEC-mediated viral restriction: Not simply editing? *Trends Biochem Sci* 32:118–128.
2. Wedekind JE, Dance GS, Sowden MP, Smith HC (2003) Messenger RNA editing in mammals: New members of the APOBEC family seeking roles in the family business. *Trends Genet* 19:207–216.
3. Sheehy AM, Gaddis NC, Choi JD, Malim MH (2002) Isolation of a human gene that inhibits HIV-1 infection and is suppressed by the viral Vif protein. *Nature* 418:646–650.
4. Conticello SG, Harris RS, Neuberger MS (2003) The Vif protein of HIV triggers degradation of the human antiretroviral DNA deaminase APOBEC3G. *Curr Biol* 13:2009–2013.
5. Marin M, Rose KM, Kozak SL, Kabat D (2003) HIV-1 Vif protein binds the editing enzyme APOBEC3G and induces its degradation. *Nat Med* 9:1398–1403.
6. Mehle A, et al. (2004) Vif overcomes the innate antiviral activity of APOBEC3G by promoting its degradation in the ubiquitin-proteasome pathway. *J Biol Chem* 279:7792–7798.
7. Sheehy AM, Gaddis NC, Malim MH (2003) The antiretroviral enzyme APOBEC3G is degraded by the proteasome in response to HIV-1 Vif. *Nat Med* 9:1404–1407.
8. Stopak K, de Noronha C, Yonemoto W, Greene WC (2003) HIV-1 Vif blocks the antiviral activity of APOBEC3G by impairing both its translation and intracellular stability. *Mol Cell* 12:591–601.

9. Yu X, et al. (2003) Induction of APOBEC3G ubiquitination and degradation by an HIV-1 Vif-Cul5-SCF complex. *Science* 302:1056–1060.
10. Henriet S, et al. (2009) Tumultuous relationship between the human immunodeficiency virus type 1 viral infectivity factor (Vif) and the human APOBEC-3G and APOBEC-3F restriction factors. *Microbiol Mol Biol Rev* 73:211–232.
11. Goila-Gaur R, Strebel K (2008) HIV-1 Vif, APOBEC, and intrinsic immunity. *Retrovirology* 5:51.
12. Iwatani Y, et al. (2007) Deaminase-independent inhibition of HIV-1 reverse transcription by APOBEC3G. *Nucleic Acids Res* 35:7096–7108.
13. Miyagi E, et al. (2007) Enzymatically active APOBEC3G is required for efficient inhibition of human immunodeficiency virus type 1. *J Virol* 81:13346–13353.
14. Bishop KN, et al. (2008) APOBEC3G inhibits elongation of HIV-1 reverse transcripts. *PLoS Pathog* 4:e1000231.
15. Nathans R, et al. (2008) Small-molecule inhibition of HIV-1 Vif. *Nat Biotechnol* 26:1187–1192.
16. Hershko A, Ciechanover A (1998) The ubiquitin system. *Annu Rev Biochem* 67:425–479.
17. Pickart CM (2001) Mechanisms underlying ubiquitination. *Annu Rev Biochem* 70:503–533.
18. Skowyra D, et al. (1997) F-box proteins are receptors that recruit phosphorylated substrates to the SCF ubiquitin-ligase complex. *Cell* 91:209–219.
19. Mehle A, et al. (2004) Phosphorylation of a novel SOCS-box regulates assembly of the HIV-1 Vif-Cul5 complex that promotes APOBEC3G degradation. *Genes Dev* 18:2861–2866.
20. Stanley BJ, et al. (2008) Structural insight into the human immunodeficiency virus Vif SOCS box and its role in human E3 ubiquitin ligase assembly. *J Virol* 82:8656–8663.
21. Kobayashi M, et al. (2005) Ubiquitination of APOBEC3G by an HIV-1 Vif-Cullin5-Elongin B-Elongin C complex is essential for Vif function. *J Biol Chem* 280:18573–18578.
22. Mehle A, Thomas ER, Rajendran KS, Gabuzda D (2006) A zinc-binding region in Vif binds Cul5 and determines cullin selection. *J Biol Chem* 281:17259–17265.
23. Xiao Z, et al. (2006) Assembly of HIV-1 Vif-Cul5 E3 ubiquitin ligase through a novel zinc-binding domain-stabilized hydrophobic interface in Vif. *Virology* 349:290–299.
24. Pery E, Rajendran KS, Brazier AJ, Gabuzda D (2009) Regulation of APOBEC3 proteins by a novel YXXL motif in human immunodeficiency virus type 1 Vif and simian immunodeficiency virus SIVagm Vif. *J Virol* 83:2374–2381.
25. Russell RA, et al. (2009) Distinct domains within APOBEC3G and APOBEC3F interact with separate regions of human immunodeficiency virus type 1 Vif. *J Virol* 83:1992–2003.
26. Schröfelbauer B, Senger T, Manning G, Landau NR (2006) Mutational alteration of human immunodeficiency virus type 1 Vif allows for functional interaction with nonhuman primate APOBEC3G. *J Virol* 80:5984–5991.
27. Bogerd HP, Doehle BP, Wiegand HL, Cullen BR (2004) A single amino acid difference in the host APOBEC3G protein controls the primate species specificity of HIV type 1 virion infectivity factor. *Proc Natl Acad Sci USA* 101:3770–3774.
28. Mangeat B, Turelli P, Liao S, Trono D (2004) A single amino acid determinant governs the species-specific sensitivity of APOBEC3G to Vif action. *J Biol Chem* 279:14481–14483.
29. Schröfelbauer B, Chen D, Landau NR (2004) A single amino acid of APOBEC3G controls its species-specific interaction with virion infectivity factor (Vif). *Proc Natl Acad Sci USA* 101:3927–3932.
30. Xu H, et al. (2004) A single amino acid substitution in human APOBEC3G antiretroviral enzyme confers resistance to HIV-1 virion infectivity factor-induced depletion. *Proc Natl Acad Sci USA* 101:5652–5657.
31. Huthoff H, Malim MH (2007) Identification of amino acid residues in APOBEC3G required for regulation by human immunodeficiency virus type 1 Vif and Virion encapsidation. *J Virol* 81:3807–3815.
32. Holden LG, et al. (2008) Crystal structure of the anti-viral APOBEC3G catalytic domain and functional implications. *Nature* 456:121–124.
33. Prochnow C, et al. (2007) The APOBEC-2 crystal structure and functional implications for the deaminase AID. *Nature* 445:447–451.
34. Eswar N, et al. (2006) Comparative protein structure modeling using Modeller. *Curr Protoc Bioinformatics* Chapter 5:Unit 5 6.
35. Kao S, et al. (2003) The human immunodeficiency virus type 1 Vif protein reduces intracellular expression and inhibits packaging of APOBEC3G (CEM15), a cellular inhibitor of virus infectivity. *J Virol* 77:11398–11407.
36. Xu H, et al. (2007) Stoichiometry of the antiviral protein APOBEC3G in HIV-1 virions. *Virology* 360:247–256.
37. Chen KM, et al. (2008) Structure of the DNA deaminase domain of the HIV-1 restriction factor APOBEC3G. *Nature* 452:116–119.
38. Furukawa A, et al. (2009) Structure, interaction and real-time monitoring of the enzymatic reaction of wild-type APOBEC3G. *EMBO J* 28:440–451.
39. Harjes E, et al. (2009) An extended structure of the APOBEC3G catalytic domain suggests a unique holoenzyme model. *J Mol Biol* 389:819–832.
40. Huthoff H, et al. (2009) RNA-dependent oligomerization of APOBEC3G is required for restriction of HIV-1. *PLoS Pathog* 5:e1000330.
41. Zhang KL, et al. (2007) Model structure of human APOBEC3G. *PLoS ONE* 2:e378.
42. Dang Y, Siew LM, Zheng YH (2008) APOBEC3G is degraded by the proteasomal pathway in a Vif-dependent manner without being polyubiquitylated. *J Biol Chem* 283:13124–13131.
43. Gooch BD, Cullen BR (2008) Functional domain organization of human APOBEC3G. *Virology* 379:118–124.
44. Zheng N, et al. (2002) Structure of the Cul1-Rbx1-Skp1-F boxSkp2 SCF ubiquitin ligase complex. *Nature* 416:703–709.
45. Scherer DC, et al. (1995) Signal-induced degradation of I kappa B alpha requires site-specific ubiquitination. *Proc Natl Acad Sci USA* 92:11259–11263.
46. Stroschein SL, Bonni S, Wrana JL, Luo K (2001) Smad3 recruits the anaphase-promoting complex for ubiquitination and degradation of SnoN. *Genes Dev* 15:2822–2836.
47. Orlicky S, et al. (2003) Structural basis for phosphodependent substrate selection and orientation by the SCFCdc4 ubiquitin ligase. *Cell* 112:243–256.
48. Iwatani Y, Takeuchi H, Strebel K, Levin JG (2006) Biochemical activities of highly purified, catalytically active human APOBEC3G: Correlation with antiviral effect. *J Virol* 80:5992–6002.

Supporting Information

Iwatani et al. 10.1073/pnas.0906652106

SI Text

Plasmids and Antibodies. A3G expression plasmids were constructed using pcDNA-A3G that contains a C-terminal MycHIS tag (consisting of Myc and $(His)_6$ (HIS) epitopes) (1, 2). Arg substitutions for A3G Lys residues and the two Lys residues in the C-terminal tag (Lys-free MycHIS tag), as well as Gln substitution for Glu-259 at the A3G catalytic center were introduced into pcDNA-A3G by using the QuikChange XL Site Directed Mutagenesis Kit (Stratagene). For all mutants, the nucleotide sequences of both the insert and the boundary regions were verified by DNA sequencing. pcDNA-HVif, a human codon-optimized clone used for Vif expression (3), was a generous gift from Dr. Klaus Strebel (NIAID, NIH).

A3G's sensitivity toward HIV-2 and SIV_{mac} Vif was tested using the appropriate expression plasmids: *vif*(+) plasmids, pGH-123 (4) and pMA239 (5), respectively; and *vif*(-) control plasmids, pGH-Xb (4) and pMA-Sc (5), respectively (generously provided by Dr. Akio Adachi, University of Tokushima). In connection with construction of a SupT1 cell line that stably expresses A3G (see below), A3G cDNA fragments were inserted into the plasmid, pRetroX-Tight-Pur (Clontech) using NotI and *Mlu*I restriction sites. The resulting plasmids that express A3G WT, S-A3G, and A3G D128K (without a tag), were designated as pRetroX A3G WT, pRetroX S-A3G, and pRetroX A3G D128K, respectively. To produce virus that can be pseudotyped with the Vesicular Stomatitis virus *env* gene (VSV-G), the clone pNLuc*vif*(-) was constructed using the luciferase-expressing, HIV-1 *env*-negative pNL4–3 derivative, pNLuc (generous gift from Dr. Eric O. Freed, NIH, NCI-Frederick) (6), and pNL4–3*vif*(-).

A peptide antibody (C-17 rabbit serum) against human A3G, anti-Vif antibody, and anti-p24 (CA) rabbit serum were obtained from the AIDS Research and Reference Reagent Program, catalog no. 10082, 2221, and 4250, respectively. Anti-Myc tag mAb (9B11, Cell Signaling Technology), anti-HIS tag rabbit serum (Medical & Biological Laboratories Co.), and β-tubulin rabbit polyclonal antibody (Abcam) were purchased from the respective companies.

Preparation of SupT1 Cells Stably Expressing A3G. For efficient expression of A3G in T-cell lymphocytes, it was necessary to construct SupT1 cells that stably express A3G. These cells were generated using the retroviral gene transfer system "Retro-X Tet-Off Advanced inducible Expression System" (Clontech), following the manufacturer's protocol. Briefly, retroviral vectors were produced by cotransfection of 293T cells with pVSV-G (Clontech), the murine leukemia virus Gag/Pol expression plasmid pMLVg/p (7), and pRetroX-Tight-Pur vector-based A3G expression plasmids or the empty vector. In addition, a retroviral vector for expression of Tet-Off transactivator was prepared by cotransfection of 293T cells with pVSV-G, pMLVg/p, and pRetro-X-Tet-Off Advanced (Clontech). SupT1 cells were serially infected with the retroviral vector for the Tet-Off transactivator and subsequently, with the A3G vector. Cells that were resistant to both G418 (500 ng/mL) (Roche) and Puromycin (1 mg/mL) were selected and doubly transfected stable cell lines expressing no A3G, A3G WT, A3G D128K, and S-A3G were designated as SupTetOff, SupTetOff A3G WT, SupTetOff A3G D128K, and SupTetOff S-A3G, respectively.

Assay of Vif-Dependent Degradation of A3G. A3G or mutant A3G expression plasmids (2 μg) and pcDNA-HVif or pcDNA 3.1 (-) control (i.e., empty) vector (4 μg) were cotransfected into Human Embryonic Kidney cells (293T) in 6-well plates, using FuGENE HD (Roche). Forty-eight hours post transfection, cell lysates were prepared in Laemmli buffer (Bio-Rad) containing 2.5% 2-mercaptoethanol (ME). Cell lysates were subjected to SDS/PAGE and the proteins were transferred to Immobilon-P membranes (Millipore). The membranes were first incubated with appropriate antibodies, as specified, and were then incubated with horseradish peroxidase-conjugated secondary antibodies (Pierce). Proteins were visualized by enhanced chemiluminescence, using SuperSignal West Dura (Pierce).

For Vif-dependent degradation of A3G in T-lymphocytes, SupTetOff cells expressing A3G (1×10^5 cells) were infected with VSV-G pseudotyped viruses (200 ng); NL4–3 WT or NL4–3 vif(-) were produced by cotransfection of 293T cells with pVSV-G and either pNLuc or pNLuc *vif*(-). At 72 h post infection, cell lysates were prepared and A3G expression was evaluated by Western blot analysis.

Detection of Polyubiquitinated A3G. 293T cells were cotransfected with A3G expression plasmid (Lys-free MycHIS tag) and pcDNA-HVif, plus either myc-tagged ubiquitin (Ub) or the mutant K48R (Arg substitution at Ub residue Lys-48) (8). Forty-eight hours post transfection, cells were lysed with 6M urea in PBS, the expressed A3G was pulled-down using TALON resin (Clontech) and proteins were detected by Western blot analysis using anti-A3G antibody.

Infectivity Assays Using LuSIV Cells. Virus production and analysis of virus infectivity were performed as reported previously (1). Briefly, to obtain virus particles, 293T cells were cotransfected with 4 μg of pNL4–3 WT and/or pNL4–3*vif*(-) (ratios as described in the main text) plus 2 μg of pcDNA-A3G or pcDNA 3.1 (-) (vector control). Virus infectivity was determined by single-cycle replication assays with LuSIV cells (9), obtained from the AIDS Research and Reference Reagent Program, NIAID, NIH (cells originally from Drs. J. W. Roos and J. E. Clements). Infectivity was calculated by normalizing for the amount of input CA, determined as p24 antigen by ELISA (ZeptoMetrix).

Incorporation of A3G into Virions. Cell-free-filtered supernatants from transfected 293T cells were pelleted (75 min, 151,000 × *g*) through a 20% sucrose cushion in an SW41 rotor, as previously described (1). The concentrated virus pellet was lysed in 1X Laemmli buffer containing 2-ME. Proteins were separated by SDS/PAGE (10% polyacrylamide gel) and were detected by immunoblotting with the appropriate antibodies.

1. Iwatani Y, Takeuchi H, Strebel K, Levin JG (2006) Biochemical activities of highly purified, catalytically active human APOBEC3G: Correlation with antiviral effect. *J Virol* 80:5992–6002.
2. Kao S, et al. (2003) The human immunodeficiency virus type 1 Vif protein reduces intracellular expression and inhibits packaging of APOBEC3G (CEM15), a cellular inhibitor of virus infectivity. *J Virol* 77:11398–11407.
3. Nguyen KL, et al. (2004) Codon optimization of the HIV-1 *vpu* and *vif* genes stabilizes their mRNA and allows for highly efficient Rev-independent expression. *Virology* 319:163–175.
4. Shibata R, et al. (1990) Mutational analysis of the human immunodeficiency virus type 2 (HIV-2) genome in relation to HIV-1 and simian immunodeficiency virus SIV (AGM). *J Virol* 64:742–747.

5. Shibata R, et al. (1991) Generation of a chimeric human and simian immunodeficiency virus infectious to monkey peripheral blood mononuclear cells. *J Virol* 65:3514–3520.
6. Kiernan RE, Ono A, Englund G, Freed EO (1998) Role of matrix in an early postentry step in the human immunodeficiency virus type 1 life cycle. *J Virol* 72:4116–4126.
7. Abudu A, et al. (2006) Murine retrovirus escapes from murine APOBEC3 via two distinct novel mechanisms. *Curr Biol* 16:1565–1570.
8. Mehle A, et al. (2004) Vif overcomes the innate antiviral activity of APOBEC3G by promoting its degradation in the ubiquitin-proteasome pathway. *J Biol Chem* 279:7792–7798.
9. Roos JW, et al. (2000) LuSIV cells: A reporter cell line for the detection and quantitation of a single cycle of HIV and SIV replication. *Virology* 273:307–315.

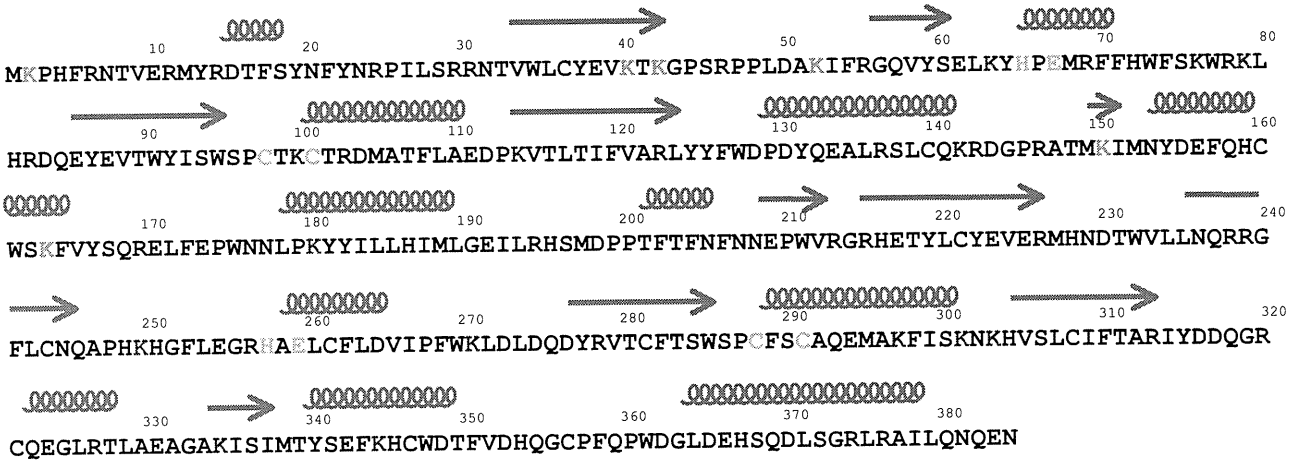

Fig. S1. Amino acid sequence of A3G. All 20 Lys residues are shown in blue, with the 14 most exposed amino acids in dark blue. The zinc-coordinating residues are colored orange. Every tenth amino acid is numbered and secondary structure elements are depicted above the sequence, with α-helices as coils and β-strands as arrows.

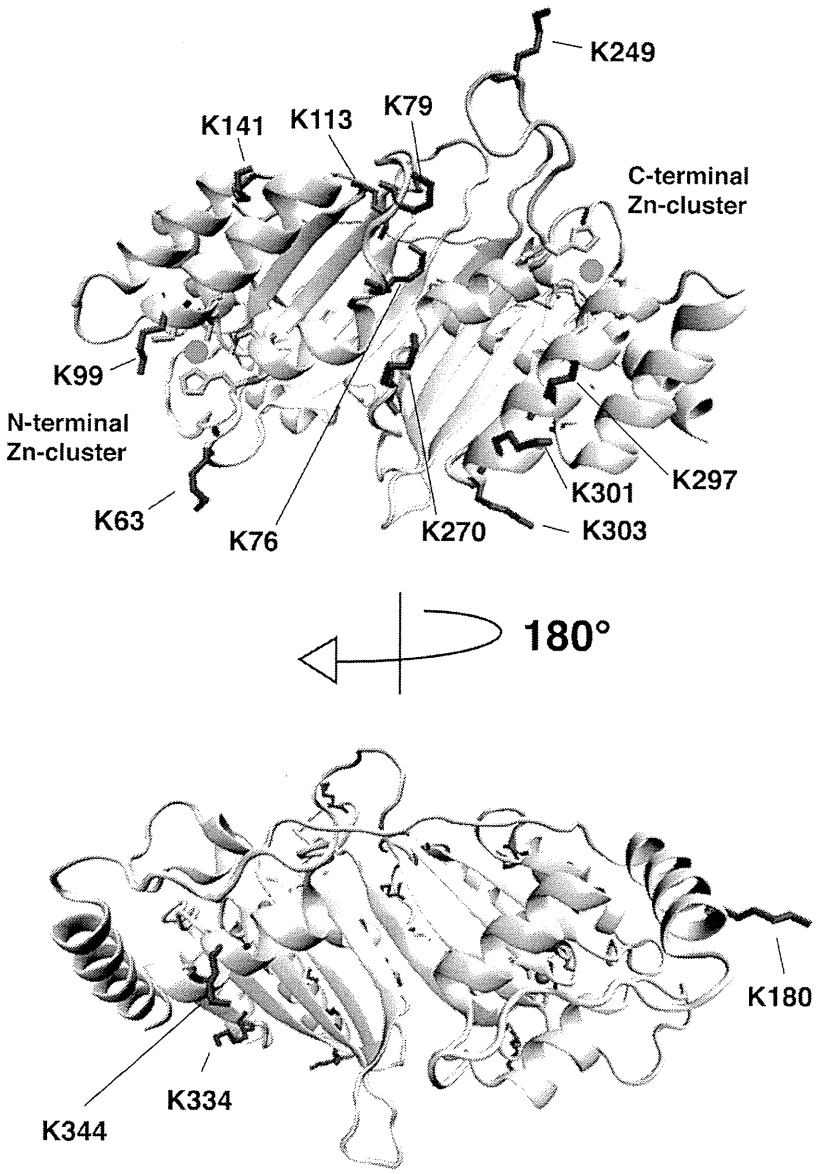

Fig. S2. Model structure of A3G. Ribbon diagram of full-length A3G in two different orientations with the side chains of the 14 most surface-exposed Lys depicted in stick representation (blue). The side chains of the Zn-coordinating residues in the NTD and CTD are also displayed and colored in orange and yellow, respectively. Positions of the zinc atoms are labeled by red spheres.

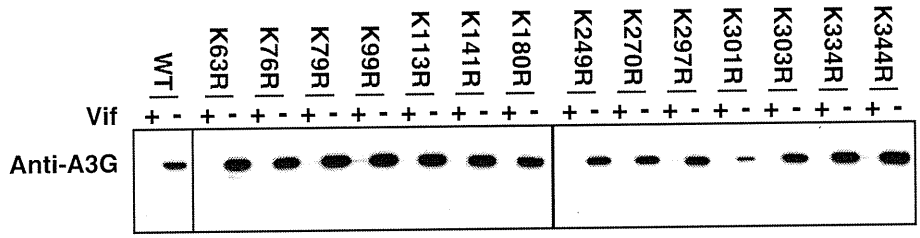

Fig. S3. Effect of single point mutations changing each of the 14 Lys residues to Arg on HIV-1 Vif sensitivity. Fourteen point mutants (K63R, K76R, K79R, K99R, K113R, K141R, K180R, K249R, K270R, K297R, K301R, K303R, K334R, and K344R) were constructed and assayed for A3G expression in the presence (+) or absence (−) of Vif, as described in the *SI Text*.

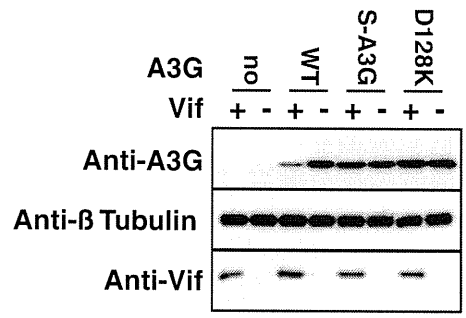

Fig. S4. Resistance of S-A3G to Vif-mediated degradation in SupT1 cells. SupT1 cells that stably express no A3G, A3G WT, S-A3G, or A3G D128K (SupTetOff, SupTetOff A3G WT, SupTetOff S-A3G, or SupTetOff A3G D128K, respectively) were prepared and infected with either VSV-G pseudotyped HIV-1 (+) or *vif*-deficient HIV-1 (−) viruses, as described in the *SI Text*. Protein expression in the absence or presence of Vif was assayed by Western blot analysis.

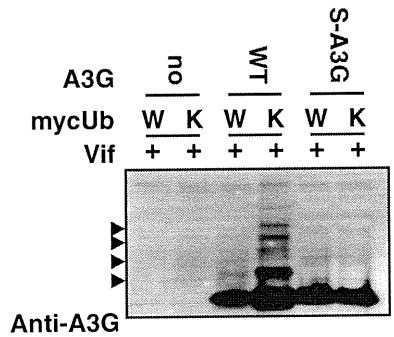

Fig. S5. Polyubiquitination of A3G mutants. 293T cells were cotransfected with Vif and the indicated A3G expression plasmids (Lys-free MycHIS tagged versions) plus either myc-tagged Ub (W) or the mutant K48R (K) expression plasmids. Ubiquitinated A3G proteins were pulled-down with TALON beads and detected by Western blot analysis using anti-A3G antibody. The positions of ubiquitinated A3G are indicated by the arrow heads.